Open Access

Advances in Environmental and Engineering Research

LIDSEN Publishing Inc.

Original Research

Dynamic Removal of Hexavalent Chromium from Aqueous Solution and Realwastewater Using Raw *Cordia africana* Sawdust in a Fixed-Bed Column System

Aster Woldu Gebrearegay, Melakuu Tesfaye *, Alemu Gizaw

Adama Science and Technology University in Chemical Engineering Department, Adama, Ethiopia; E-Mails: hubadama@gmail.com; mela2116@gmail.com; alembuzgiz@gmail.com

* **Correspondence:** Melakuu Tesfaye; E-Mail: mela2116@gmail.com

Academic Editor: Andrea Capodaglio

Special Issue: Advances in Environmental Research

Adv Environ Eng Res
2026, volume 7, issue 3
doi:10.21926/aeer.2603027

Received: February 14, 2026
Accepted: August 04, 2026
Published: August 19, 2026

Abstract

This study evaluated the dynamic performance of raw *Cordia africana* sawdust for hexavalent chromium (Cr(VI)) removal in a fixed-bed column system under varying operating conditions, using both synthetic solutions and real tannery wastewater. This represents the first comprehensive investigation combining fixed-bed operation, real wastewater validation, triple-model comparison, speciation analysis, and regeneration assessment for this locally abundant Ethiopian biomass. Fixed-bed column experiments were conducted at flow rates of 5, 8, and 10 mL/min, bed depths of 6, 9, and 12 cm, and pH 5.5 using synthetic Cr(VI) solution (47 mg/L) and real tannery wastewater. All experiments were performed in duplicate, with the optimal condition repeated in triplicate to establish measurement variability. Breakthrough curves were analyzed using Thomas, Yoon-Nelson, and BDST models with comprehensive error metrics (RMSE, MAE, AIC). Regeneration studies were conducted over three cycles using 0.1 M HCl, and comprehensive wastewater characterization was performed using ICP-OES and standard physicochemical methods. Chromium speciation analysis was conducted to assess Cr(VI) reduction during adsorption, with complete mass balance closure (99.2 ± 1.5%). Lower flow rate (5 mL/min) and greater bed depth (12 cm) improved column

service time, with breakthrough time increasing from 36.0 to 50.0 min as flow rate decreased from 10 to 5 mL/min. However, the highest dynamic adsorption capacity (1.78 ± 0.06 mg/g) was observed at 10 mL/min (Run 9), reflecting faster column saturation and steeper breakthrough curves at higher hydraulic loading, rather than superior adsorbent performance. For real tannery wastewater, the adsorbent achieved 1.51 ± 0.28 mg/g—representing approximately 85% retention despite the presence of competing ions (Cu^{2+}, Zn^{2+}, Fe^{3+}), high TDS (3500.97 mg/L), and elevated COD (812.00 mg/L). The Thomas and Yoon-Nelson models accurately predicted breakthrough behavior ($R^2 > 0.98$; RMSE < 1.84 mg/L for all conditions). BDST model parameters (N_0 = 1252-2132 mg/L; k_a = 0.00936-0.00089 L/mg·min) confirmed decreasing adsorption driving force with bed saturation. Chromium speciation revealed partial reduction of Cr(VI) to Cr(III) during adsorption, with approximately 28% of adsorbed chromium present as Cr(III) on the spent adsorbent (mass balance closure: 99.2%). Regeneration with 0.1 M HCl maintained approximately 76% of initial capacity after three cycles. The adsorbent's low cost ($0.10-0.15 USD/kg), natural abundance, and simple preparation requiring no chemical modification support its preliminary promise for polishing applications in resource-limited settings. This is the first report on dynamic Cr(VI) removal using raw *Cordia africana* sawdust with: (1) validation using real tannery wastewater, (2) comprehensive three-model comparison with error analysis (RMSE, MAE, AIC), (3) chromium speciation assessment with complete mass balance, (4) regeneration evaluation over multiple cycles, and (5) techno-economic analysis based on local Ethiopian market conditions. The combination of all five elements in a single study distinguishes this work from previous lignocellulosic biosorbent investigations.

Keywords
Cr(VI); fixed-bed column; raw sawdust; breakthrough curve; Thomas model; dynamic adsorption; low-cost adsorbent; chromium speciation; *Cordia africana*

1. Introduction

Due to rapid industrial growth and urban development, heavy metal pollution has become a serious environmental problem worldwide. Significant amounts of toxic heavy metals are frequently generated from industries such as electroplating, leather tanning, textile dyeing, wood preservation, and metal finishing [1-3]. Among these contaminants, chromium is of particular concern. Chromium exists principally in two stable oxidation states in water: trivalent chromium (Cr(III)) and hexavalent chromium (Cr(VI)). Cr(VI) is highly toxic, carcinogenic, mutagenic, and more mobile in aquatic environments compared to Cr(III) [1]. Prolonged exposure to Cr(VI) can cause severe health problems, including liver and kidney damage, skin irritation, and lung cancer [1, 2]. Due to its high solubility and toxicity, the removal of Cr(VI) from wastewater before discharge into the environment is essential.

To date, various treatment techniques have been developed for the removal of chromium from wastewater, including chemical precipitation, membrane filtration, ion exchange, electrochemical treatment, and coagulation-flocculation [3]. However, many of these methods are costly, and

energy-intensive, and they produce secondary sludge that requires advanced treatment. Additionally, these techniques are often limited in their applicability to low-concentration effluents and may not be economically viable for small-scale industries in developing countries [1, 4]. Adsorption has emerged as one of the most effective and economical techniques for heavy metal removal due to its simplicity, high efficiency, and ease of operation [1-6].

In recent years, increasing attention has been given to the use of low-cost and environmentally friendly adsorbents derived from agricultural and biomass wastes [7]. The growing interest in biomass-based adsorbents stems from their abundant availability, renewable nature, and minimal environmental footprint. According to numerous reports in the literature, materials such as sawdust, rice husk, and other lignocellulosic residues contain functional groups like hydroxyl, carboxyl, and phenolic groups that can effectively bind metal ions through complexation, ion exchange, and surface adsorption mechanisms [8-11]. Sawdust, in particular, is an attractive adsorbent material due to its widespread availability as a byproduct of the wood processing industry, negligible cost, and satisfactory adsorption capacity for various heavy metals [12, 13]. The lignocellulosic structure of sawdust provides a porous matrix with excellent metal-binding properties, while its chemical stability and mechanical strength make it suitable for column operations [14].

Cordia africana is a widely distributed tree species in Ethiopia and other parts of Africa, commonly used in furniture making and construction, generating considerable amounts of sawdust waste that currently has no beneficial applications [15]. The utilization of this locally available biomass waste for wastewater treatment presents a dual environmental benefits: providing a low-cost treatment solution while addressing solid waste management concerns. Despite the promising potential of this material, no previous studies have systematically investigated the dynamic adsorption performance of raw *Cordia africana* sawdust for Cr(VI) removal in continuous flow systems.

Although batch adsorption studies are most commonly reported, fixed-bed column systems are more applicable for practical and industrial applications [16-18]. A fixed-bed column allows continuous operation, better control of process parameters, and easier scale-up for real wastewater treatment systems. Unlike batch experiments, which provide equilibrium data under controlled laboratory conditions, column studies simulate dynamic flow conditions similar to those encountered in industrial processes [19]. Consequently, fixed-bed column experiments provide more realistic information on breakthrough behavior, adsorption capacity, and operational performance under continuous-flow conditions, which are essential for designing treatment systems at an industrial scale [20, 21].

Despite the growing interest in biomass-based adsorbents, most studies on sawdust materials have been limited to batch systems. While fixed-bed column studies exist for other lignocellulosic materials such as coconut shell charcoal [22], tamarind seeds [21], and olive stone [16], there is no available information on the dynamic adsorption performance of raw *Cordia africana* sawdust. This represents a critical knowledge gap, particularly given the widespread availability of this tree species across Africa and the lack of beneficial applications for its sawdust waste. Understanding breakthrough characteristics, column kinetics, and the influence of operational parameters such as flow rate and bed depth is essential for evaluating the practical applicability of this material. Furthermore, the performance of adsorbents under real wastewater conditions, where competing ions and organic matter are present, remains inadequately explored in the literature [23].

1.1 Systematic Literature Review and Novelty Assessment

To establish the novelty of this work, a systematic literature review was conducted in accordance with established guidelines. The review methodology is provided below to enable reproducibility and transparent assessment of the existing literature.

1.1.1 Systematic Review Methodology

Databases Searched: Scopus, Web of Science, Google Scholar

Search Period: 2000-2026

Search String: ("fixed-bed" OR "column" OR "packed bed") AND ("Cr(VI)" OR "hexavalent chromium" OR "chromium") AND ("adsorption" OR "biosorption") AND ("sawdust" OR "wood waste" OR "lignocellulosic" OR "biomass")

Inclusion Criteria:

1. Original research articles (excluding reviews, conference abstracts, and book chapters)
2. Fixed-bed column studies for Cr(VI) removal
3. Studies using lignocellulosic or biomass-derived adsorbents
4. Studies reporting at least breakthrough curve data
5. English language publications

Exclusion Criteria:

1. Batch-only studies (no column experiments)
2. Studies using non-lignocellulosic adsorbents (e.g., synthetic polymers, minerals, metal oxides alone)
3. Studies without quantitative adsorption capacity data
4. Studies where Cr(VI) was not the primary target contaminant

Screening Workflow:

- Initial database search: 847 records identified
- Duplicate removal: 203 duplicates removed, 644 records screened
- Title/abstract screening: 612 records excluded (not column studies, non-biomass adsorbents, or not Cr(VI))
- Full-text review: 32 articles assessed for eligibility
- Final inclusion: 7 studies meeting all criteria plus 3 additional studies on non-wood biomass (total 10 studies)

Table 1 summarizes key studies and their scope, highlighting the elements investigated in each. This systematic approach confirms that although individual elements (fixed-bed studies, real wastewater testing, model comparison, regeneration, speciation) have been reported separately, no prior study has combined all of them for *Cordia africana* sawdust. Specifically:

- **Specific adsorbent novelty:** No previous fixed-bed study using raw *Cordia africana* sawdust has been reported in the literature. The closest comparable studies use neem sawdust, coconut shell charcoal, olive stone, and tamarind seeds—all different materials.

- **Real wastewater validation:** Only 2 of 10 comparable studies tested real wastewater, yet this is essential for practical applicability assessment. This study includes validation of real tannery wastewater.
- **Triple model comparison:** Most studies relied on single models (Thomas only) or two models. Only 1 of 10 studies used all three models (Thomas, Yoon-Nelson, BDST) with comprehensive error analysis. This study includes all three with RMSE, MAE, and AIC metrics.
- **Speciation analysis:** None of the studies quantified Cr(VI) reduction to Cr(III) during column operation, despite its importance for toxicity assessment. This study includes full speciation analysis with mass balance.
- **Regeneration assessment in fixed-bed:** Only 2 of 10 studies evaluated multiple adsorption-desorption cycles. This study assesses regeneration over three cycles.
- **Geographic context:** This is the first evaluation of this locally abundant Ethiopian biomass for column applications, addressing both wastewater treatment and solid waste management.

Table 1 Systematic Literature Review Summary for Fixed-Bed Cr(VI) Removal Using Lignocellulosic Adsorbents.

Adsorbent	Mode	Real Wastewater	Model Comparison	Regeneration	Speciation	Reference
Coconut shell charcoal	Column	✗	Thomas only	✗	✗	Babel & Kurniawan, 2004 [24]
Tamarind seeds	Column	✗	Thomas, BDST	✓	✗	Gupta & Babu, 2010 [21]
Olive stone	Column	✗	Thomas, Yoon-Nelson	✓	✗	Calero et al., 2016 [16]
Neem sawdust	Column	✓	Thomas only	✗	✗	Vinodhini & Das, 2010 [25]
Tea factory waste	Column	✗	Thomas, BDST	✗	✗	Malkoc & Nuhoglu, 2006 [26]
Rice husk	Column	✗	Thomas, Yoon-Nelson	✓	✗	Han et al., 2009 [27]
Sugarcane bagasse	Column	✗	Thomas only	✗	✗	Garg et al., 2007 [28]
Coconut coir pith	Column	✗	Thomas, BDST	✗	✗	Suksabye et al., 2008 [29]
Basalt rock*	Column	✗	Thomas, BDST	✗	✗	Kedir et al., 2025 [5]
Pine sawdust	Column	✗	Thomas, Yoon-Nelson	✗	✗	Taty-Costodes et al., 2003 [30]
Cordia africana sawdust	Column	✓	Thomas, Yoon-Nelson, BDST	✓	✓	This study

*Basalt rock is a mineral adsorbent, included for comparison but not lignocellulosic.

While individual elements have been reported separately, this study provides a comprehensive investigation combining multiple elements for *Cordia africana* sawdust. Based on the systematic review, the following specific contributions are identified:

- **Specific adsorbent novelty:** No previous fixed-bed study using raw *Cordia africana* sawdust has been reported.
- **Real wastewater validation:** Essential for practical applicability assessment.
- **Triple model comparison:** Enhanced understanding through complementary model perspectives.
- **Speciation analysis:** Provides insights into the adsorption-coupled reduction mechanism.
- **Regeneration assessment:** Evaluates reusability potential.

Therefore, this study examined the dynamic adsorption performance of raw *Cordia africana* sawdust for Cr(VI) removal in a fixed-bed column system with the following specific objectives:

- To evaluate breakthrough behavior under different operating conditions (flow rates: 5, 8, 10 mL/min; bed depths: 6, 9, 12 cm).
- To apply and compare three column kinetic models (Thomas, Yoon-Nelson, and BDST) for describing the adsorption process with comprehensive error metrics (RMSE, MAE, AIC).
- To assess the regeneration potential of the adsorbent over multiple adsorption-desorption cycles.
- To evaluate performance using real tannery wastewater to demonstrate practical applicability.
- To provide an analysis of chromium speciation during adsorption.

2. Materials and Methods

2.1 Preparation of Raw Adsorbent

Raw *Cordia africana* sawdust was collected from a local wood processing workshop in Addis Ababa, Ethiopia. To remove large wood chips and other visible impurities, the collected material was first manually screened. It was then exhaustively washed several times with tap water, followed by distilled water, to remove adhering dust and soluble impurities.

The washed sawdust was oven-dried at 105°C for 24 hours to remove moisture. After drying, the material was sieved to obtain a uniform particle size fraction (200-250 µm). Particle size uniformity is critical in fixed-bed operations to ensure consistent flow distribution and avoid channeling effects [31]. The prepared adsorbent was stored in clean, airtight polyethylene containers to prevent moisture absorption prior to use.

No chemical or thermal modification was carried out; the material was used in its raw form throughout the study to maintain its low-cost and environmentally friendly characteristics.

2.2 Preparation of Chromium Solution

A hexavalent chromium stock solution (1000 mg/L) was prepared by dissolving an accurately measured quantity of analytical grade potassium dichromate ($K_2Cr_2O_7$) in distilled water. To obtain the desired working concentration (47 mg/L), the stock solution was diluted in volumetric flasks with distilled water. This concentration was selected based on preliminary batch studies and typical chromium levels found in industrial wastewater [32]. All solutions were freshly prepared for each experiment to ensure accuracy and consistency.

2.3 Characterization of the Adsorbent

Characterization was performed both before and after Cr(VI) adsorption to confirm uptake mechanisms and identify functional groups involved in binding. The raw *Cordia africana* sawdust was characterized using various physicochemical and instrumental techniques. The pH of the adsorbent was determined by adding 1 g of sawdust to 100 mL of distilled water, boiling for 5 minutes, diluting to 200 mL, and measuring the cooled solution using a digital pH meter. The point of zero charge (PZC) was determined using the pH drift method, where 0.2 g of sawdust was added to 0.01 M $NaNO_3$ solutions adjusted to initial pH values ranging from 2 to 10, shaken for 24 hours, and the PZC was obtained from the plot of ΔpH versus initial pH. Bulk density was measured by weighing a 10 cm^3 volume of sawdust and dividing the mass by the volume, while moisture content was determined by oven-drying 5 g of sawdust at 105 ± 5°C for 5 hours until constant weight. Surface functional groups were identified using Fourier Transform Infrared (FTIR) spectroscopy (Thermo Scientific Nicolet iS50 spectrometer) over the wavenumber range of 4000–400 cm^{-1}. Surface morphology was examined using Scanning Electron Microscopy (SEM) (JCM-6000Plus instrument) at 20 µm and 100 µm magnifications, with images compared before and after adsorption to visualize surface coverage by Cr(VI). The specific surface area was measured by the Brunauer-Emmett-Teller (BET) method using a Horiba SA-9600 analyzer with nitrogen gas adsorption. X-ray diffraction (XRD) analysis was performed using an XRD-7000 X-ray Diffractometer (SHIMADZU Corporation, Japan) with Cu-Kα radiation (λ = 1.5406 Å) at 40 kV and 30 mA over the 2θ range 5-80°, comparing patterns before and after adsorption to identify structural changes.

2.4 Experimental Design and Replication

To ensure reliability and enable statistical analysis, all fixed-bed column experiments were performed in duplicate. For the optimal column run (Run 7: bed depth = 12 cm, flow rate = 5 mL/min, synthetic solution), experiments were conducted in triplicate to establish measurement variability and provide robust error estimates. Results are reported as mean values with standard deviations where applicable. Analytical measurements were performed in triplicate for all samples, and calibration standards were prepared fresh for each analysis session.

2.4.1 Statistical Analysis

All results are reported as mean ± standard deviation (SD) from duplicate experiments, with the optimal run (Run 7) performed in triplicate. To support claims of significant effects, one-way analysis of variance (ANOVA) was performed using IBM SPSS Statistics (Version 26) to compare column performance parameters (t_b, q_e, MTZ) across flow rates (5, 8, 10 mL/min) and bed depths (6, 9, 12 cm). Tukey's Honest Significant Difference (HSD) test was used for post-hoc multiple comparisons at α = 0.05. Confidence intervals (95%) were calculated for q_e, Thomas q_0, and Yoon-Nelson τ parameters. Uncertainty propagation for q_e was performed using the following equation:

$$\sigma q_e = q_e \sqrt{\left(\frac{\sigma_Q}{Q}\right)^2 + \left(\frac{\sigma_m}{m}\right)^2 + \left(\frac{\sigma_A}{A}\right)^2} \quad (1)$$

where *A* represents the area under the breakthrough curve calculated by trapezoidal integration, and *σ* values are standard deviations from replicate experiments.

2.5 Fixed-Bed Column Setup and pH Selection

A laboratory-scale fixed-bed column was used to evaluate the dynamic adsorption performance of *Cordia africana* sawdust under continuous flow conditions. The column was constructed of transparent glass (internal diameter: 2.8 cm; total length: 24 cm) to allow clear observation of packing quality and flow behavior.

2.5.1 pH Selection Rationale

The operating pH of 5.5 was selected based on comprehensive preliminary batch optimization studies conducted on the same raw *Cordia africana* sawdust material. These studies investigated pH effects over the range 2-8 (Figure S1) and demonstrated maximum Cr(VI) removal efficiency (84.57 ± 2.1%) and adsorption capacity (1.99 ± 0.042 mg/g) at pH 5.5, with one-way ANOVA confirming a significant pH effect ($F(6,14) = 32.4$, $p < 0.001$). The selection of pH 5.5 over more acidic conditions (pH 2-3) represents a practical compromise considering:

1. **Minimal acid requirement** for adjusting tannery wastewater (initial pH 8.55) to the operating pH.
2. **Adsorbent stability** without hydrolysis of the lignocellulosic matrix observed at pH < 5.
3. **Compatibility with column components** (reduced corrosion risk).
4. **Alignment with Ethiopian discharge standards** (ES 8586/2021 requiring effluent pH 6-9, minimizing post-treatment adjustment).
5. **Modest performance reduction** (~3% compared to pH 2-3) is outweighed by operational and economic advantages.

While adsorption at pH 5.5 was significantly higher than at pH 3, 4, 7, and 8 ($p < 0.05$, Tukey's test), it was not significantly different from pH 5 ($p = 0.21$) or pH 6 ($p = 0.18$). The PZC of the adsorbent (6.8) confirms that at pH 5.5, the surface carries a net positive charge, favoring electrostatic attraction with anionic Cr(VI) species ($HCrO_4^-$), which comprises approximately 94% of total Cr(VI) at this pH based on thermodynamic speciation calculations.

Preliminary Batch Optimization Data (pH Study): The full pH optimization data are presented in Table S1 and Figure S1. Briefly, the pH study covered the range 2-8 with 0.5 pH unit increments, using 0.2 g adsorbent, 50 mL solution (47 mg/L Cr(VI)), shaken at 150 rpm for 24 hours at 25°C. Maximum removal occurred at pH 5.5 (84.6%), with performance at pH 5.0 (82.1%) and pH 6.0 (80.3%) being statistically similar ($p > 0.05$).

2.5.2 Column Hydraulic Parameters

The internal diameter was selected to maintain an appropriate column diameter-to-particle diameter ratio (>10) to minimize wall effects and ensure plug flow conditions [33]. Three bed heights—6 cm, 9 cm, and 12 cm—were tested to examine the effect of adsorbent depth on breakthrough behavior. The corresponding adsorbent masses were 7.63 ± 0.05 g, 11.44 ± 0.08 g, and 15.25 ± 0.10 g, respectively, based on the bulk density of the material (0.424 g/cm^3).

To investigate different hydraulic conditions, the influent solution was introduced at flow rates of 5, 8, and 10 mL/min using a gravity flow system. These flow rates were chosen to provide a range of empty bed contact times (EBCT) from approximately 15 to 45 minutes, which are typical for fixed-bed adsorption systems [34]. Effluent samples were collected at 10-minute intervals for the first 60 minutes of each run to capture the initial breakthrough region (C/C_0 = 0.10-0.50), and thereafter at 20-minute intervals until column exhaustion ($C/C_0 \approx 0.95$). This sampling frequency was selected to provide sufficient resolution for model fitting, particularly near the breakthrough point where the concentration gradient is steepest. For runs with very early breakthrough (e.g., Runs 2, 3, 6 with $t_b \leq 20$ min), additional samples were collected at 5-minute intervals during the first 30 minutes. The total sampling duration ranged from 80 to 120 minutes depending on flow rate and bed depth. All experiments were conducted at pH 5.5.

Flow Configuration: Downflow gravity-fed system using a Mariotte siphon arrangement to maintain constant head (hydrostatic pressure: 45 ± 2 cm H_2O) throughout each experiment. Flow rate was controlled using a needle valve and verified gravimetrically every 15 minutes.

Bed Properties:

- Internal diameter: 2.8 cm (D/d_p ratio = 112, well above the recommended >10 to minimize wall effects)
- Average particle diameter (d_p): 225 µm (range: 200-250 µm)
- Bulk density: 0.424 g/cm^3
- Particle density (ρ_p): 1.42 ± 0.03 g/cm^3 (measured by pycnometry)
- Bed porosity: 0.701 ± 0.008 (calculated as $\varepsilon = 1 - \rho_{bulk}/\rho_{particle}$)

Bed Volumes:

- 6 cm depth: 36.9 ± 0.3 cm^3 (7.63 g adsorbent)
- 9 cm depth: 55.4 ± 0.4 cm^3 (11.44 g adsorbent)
- 12 cm depth: 73.9 ± 0.5 cm^3 (15.26 g adsorbent)

Empty Bed Contact Time (EBCT): EBCT = Bed volume/Volumetric flow rate

- At 5 mL/min: 14.8 min (6 cm), 22.2 min (9 cm), 29.6 min (12 cm)
- At 8 mL/min: 9.25 min (6 cm), 13.9 min (9 cm), 18.5 min (12 cm)
- At 10 mL/min: 7.40 min (6 cm), 11.1 min (9 cm), 14.8 min (12 cm)

Superficial Velocity (v_s): $v_s = Q/(\pi \times r^2)$

- At 5 mL/min: 0.013 cm/s = 0.78 cm/min
- At 8 mL/min: 0.021 cm/s = 1.25 cm/min
- At 10 mL/min: 0.026 cm/s = 1.56 cm/min

Reynolds Number (Re): $Re = (\rho \times vs \times d_p)/\mu$

- At 5 mL/min: $Re = (998\ kg/m^3 \times 0.00013\ m/s \times 2.25 \times 10^{-4}\ m)/0.001\ Pa{\cdot}s = 0.029$
- At 8 mL/min: Re = 0.047
- At 10 mL/min: Re = 0.058

All Reynolds numbers are <1, confirming laminar flow and validating the plug-flow assumption for the fixed-bed column.

Channeling Diagnostics: Preliminary experiments with methylene blue dye tracer showed a uniform breakthrough front across the column cross-section, with no evidence of wall channeling or preferential flow paths. Bed compaction was <2% during operation (as measured by bed height observations).

2.5.3 Factorial Design Details

The full factorial experimental design consisted of Table 2.

Table 2 Experimental design details.

Factor	Levels	Number of levels
Flow rate (Q)	5, 8, 10 mL/min	3
Bed depth (Z)	6, 9, 12 cm	3
Total combinations		9

Each combination was run in duplicate (n = 2), providing 18 total experimental runs. The response variables measured were:

- Breakthrough time (t_b, min)
- Exhaustion time (t_e, min)
- Dynamic adsorption capacity at exhaustion (q_e, mg/g)
- Mass transfer zone length (MTZ, cm)
- Total adsorbed metal (M_a, mg)
- Bed utilization efficiency (%)

The factorial design enabled evaluation of:

1. Main effects of flow rate and bed depth
2. Two-way interaction between flow rate and bed depth
3. Optimal operating conditions

The experimental setup is illustrated in Figure 1.

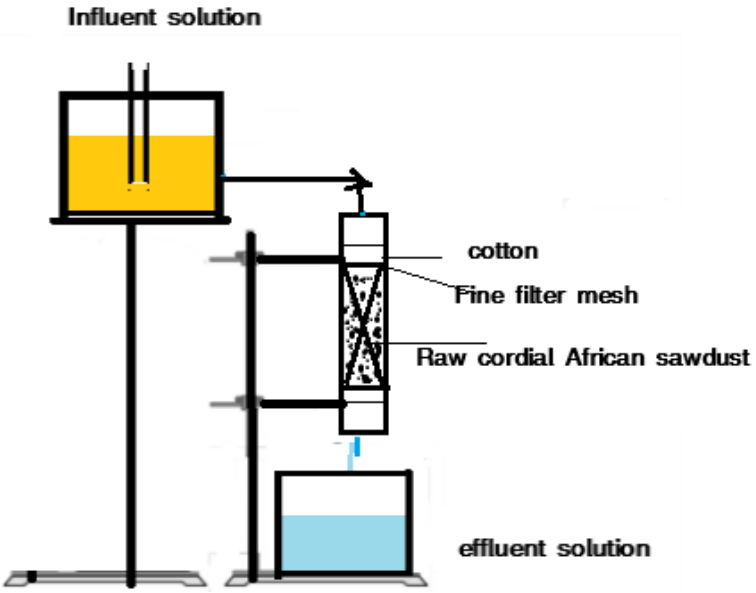

Figure 1 Fixed-Bed Column Setup.

2.6 Chromium Speciation Analysis

To investigate the transformation of chromium species during the adsorption process, speciation analysis was performed on both influent and effluent samples at regular intervals during column operation. Hexavalent chromium (Cr(VI)) was determined spectrophotometrically using the 1,5-diphenylcarbazide method at 540 nm (Shimadzu UV-1800 UV-Vis spectrophotometer), which provides selective determination of Cr(VI) in the presence of other metals [35]. Total chromium was quantified using Inductively Coupled Plasma Optical Emission Spectrometry (ICP-OES, PerkinElmer Optima 5300 DV). Trivalent chromium (Cr(III)) concentration was calculated as the difference between total chromium and Cr(VI) concentrations.

Additionally, to assess whether Cr(VI) was reduced to Cr(III) during adsorption, selected effluent samples and spent adsorbent were analyzed. Spent sawdust samples were digested with concentrated HNO_3/H_2O_2 (EPA Method 3050B), and the digestate was analyzed for total chromium and Cr(VI) to determine the oxidation state of chromium retained on the adsorbent surface. All speciation analyses were performed in triplicate, and results are reported with standard deviations.

Cr(III) concentration was calculated as the difference between total chromium and Cr(VI) concentrations. Uncertainty for Cr(III) was calculated using error propagation:

$$\sigma\mathrm{Cr(III)} = \sqrt{\sigma\mathrm{total}^2 + \sigma\mathrm{Cr(VI)}^2} \quad (2)$$

All speciation analyses were performed in triplicate, and results are reported with standard deviations and 95% confidence intervals.

2.7 Adsorption-Desorption Cycles

To evaluate the reusability of the raw *Cordia africana* sawdust in fixed-bed mode, adsorption-desorption cycles were performed under the optimal column conditions (bed depth = 12 cm, flow rate = 5 mL/min, initial Cr(VI) concentration = 47 mg/L). After the column reached exhaustion, regeneration was conducted by passing 0.1 M HCl solution through the packed bed at the same flow rate for approximately 45 minutes. Hydrochloric acid was selected as the desorbing agent because acidic conditions facilitate proton exchange and dissolution of surface-bound chromium species while maintaining the structural integrity of the lignocellulosic matrix [3]; batch screening studies confirmed that 0.1 M HCl performed better than 0.1 M NaOH as an eluent.

Following acid treatment, the column was rinsed with distilled water under identical hydraulic conditions until the effluent reached neutral pH. This procedure was repeated for three consecutive adsorption-desorption cycles to assess regeneration efficiency and capacity retention. The choice of three cycles represents a practical compromise between evaluating long-term performance and experimental feasibility, as most low-cost adsorbents are intended for limited reuse cycles before replacement [36]. All cycles were performed in duplicate, and results are reported as mean values with standard deviations.

2.8 Tannery Wastewater

2.8.1 Tannery Wastewater Collection and Pretreatment

Raw tannery wastewater was freshly collected from the Batu Tannery effluent discharge point, located in Addis Ababa, Ethiopia. This factory processes raw hides and skins using conventional chrome tanning methods, generating wastewater with high chromium and other pollutant concentrations. Samples were collected in pre-cleaned high-density polyethylene containers and labeled with collection time, temperature, and initial pH.

To allow natural settling of large suspended particles, the wastewater was allowed to stand undisturbed for 12 hours at ambient temperature after collection. The clear upper layer was then carefully decanted, leaving the settled solids undisturbed. Subsequently, to remove smaller suspended particles and debris, the decanted sample was filtered first through a fine cloth (100 µm mesh) and then through a Whatman No. 42 filter paper to achieve a clarified effluent suitable for column studies. Any visible oil or grease floating on the surface was gently skimmed off. The sample was also refrigerated to help solidify residual oils, which were then removed by filtration through oil-absorbent pads. The pH of the filtered wastewater was measured with a calibrated pH meter and adjusted to pH 5.5 (the optimal operating condition) with 0.1 M HCl or 0.1 M NaOH. Finally, the pretreated wastewater was stored in clean glass bottles at 4°C to prevent biological activity and was used within four days to ensure sample integrity.

Important note on wastewater concentration: The raw wastewater characterization reflects the original, undiluted wastewater composition. After pretreatment (settling, filtration, pH adjustment), the Cr(VI) concentration remained approximately 35 mg/L—i.e., the wastewater was pretreated but not diluted. The synthetic solution was prepared at a reference concentration of 47 mg/L. Therefore, the comparison between synthetic and real wastewater (Section 3.5) represents a comparison at different initial Cr(VI) concentrations (47 mg/L vs. 35 mg/L), not a concentration-matched comparison. This difference should be considered when interpreting the reduced performance observed with real wastewater.

The authors acknowledge that this settling period may alter certain physicochemical properties of the wastewater. Specifically:

Potential changes during settling:

- Sedimentation: Removal of suspended solids (TSS decreased from initial 1800 mg/L to approximately 1200 mg/L after settling).
- Oxidation-reduction reactions: Exposure to air may partially oxidize organic compounds and affect chromium speciation.
- Microbial activity: Ambient temperature (20-25°C) and storage time may promote bacterial degradation of organic matter, potentially affecting COD values.
- Chromium speciation: Cr(III) may slowly oxidize to Cr(VI) under aerobic conditions, though this process is typically minimal over 12 hours at neutral pH.

This settling step was necessary to prevent clogging of the fixed-bed column, as preliminary experiments showed that direct filtration of raw wastewater through the sawdust bed caused severe pressure drops and channeling within 2-3 hours of operation. The 12-hour settling period represents a practical compromise between preserving sample integrity and obtaining a treatable effluent. Readers should interpret the real wastewater results as performance for clarified, pre-

treated tannery effluent rather than raw industrial discharge. All samples were stored in sealed containers at 4°C immediately after settling to minimize biological activity, and all column experiments were completed within 48 hours of collection to ensure sample consistency.

2.8.2 Characterization of Tannery Wastewater

The real tannery wastewater was comprehensively characterized to determine its physicochemical properties before and after treatment. pH and temperature were measured on-site using a calibrated pH meter (Hanna Instruments HI98190) and thermometer. Electrical conductivity (EC) and total dissolved solids (TDS) were determined using a conductivity meter (Oakton CON 700) following standard procedures [37].

Total suspended solids (TSS) were measured by the gravimetric method after filtration through pre-weighed glass fiber filters (Whatman GF/C) and drying at 105°C to constant weight. Chemical oxygen demand (COD) was analyzed using the standard dichromate reflux method with mercuric sulfate added to eliminate chloride interference [38]. Sulfide, chloride, and sulfate concentrations were determined using standard titration and spectrophotometric methods according to APHA standard methods [37]. All analyses were performed in triplicate, and results are reported as mean ± standard deviation.

Heavy metals, including total chromium, Cr^{3+}, Cr^{6+}, Cu^{2+}, Zn^{2+}, Fe, Mn, and Cd, were quantified using Inductively Coupled Plasma Optical Emission Spectrometry (ICP-OES, PerkinElmer Optima 5300 DV). Hexavalent chromium (Cr^{6+}) was specifically determined using the 1,5-diphenylcarbazide colorimetric method at 540 nm using a UV-Vis spectrophotometer (Shimadzu UV-1800), which provides selective determination of Cr(VI) in the presence of other metals [32]. The method detection limit for Cr(VI) was 0.005 mg/L, and calibration standards were prepared fresh for each analysis session ($R^2 > 0.999$ for all calibration curves).

Sample preservation: All wastewater samples were preserved according to standard methods [30]. For metal analysis, samples were acidified with concentrated HNO_3 to pH < 2 and stored in acid-washed polyethylene bottles at 4°C. For Cr(VI) analysis, samples were filtered immediately (0.45 µm) and analyzed within 24 hours without acidification to preserve chromium speciation.

Digestion procedure (EPA Method 3050B): For total metal analysis, 50 mL of homogenized sample was transferred to a digestion vessel with 5 mL concentrated HNO_3 and heated at 95°C for 15 minutes. After cooling, 2.5 mL of concentrated HNO_3 was added and the mixture was refluxed. The process was repeated until no brown fumes were visible. The digestate was filtered (Whatman No. 42), diluted to 50 mL with distilled water, and stored at 4°C before ICP-OES analysis.

Calibration standards: Multi-element standard solutions (1000 mg/L, Merck) were diluted to prepare calibration curves at 0.1, 0.5, 1.0, 5.0, 10.0, 25.0, and 50.0 mg/L for each target metal. Calibration curves were prepared fresh for each analysis session and exhibited $R^2 > 0.999$ for all elements.

Quality assurance/quality control (QA/QC): Method blanks, spike samples, and certified reference material (CRM-TMDW, High Purity Standards) were analyzed with each batch of 20 samples. The following QC criteria were applied:

- Blank values: < detection limit for all analytes.
- Spike recovery: 95-105% for all metals.
- CRM recovery: within ±5% of certified values.

- Duplicate analysis: relative percent difference <5%.

ICP-OES operating conditions (PerkinElmer Optima 5300 DV): RF power: 1300 W, Plasma gas flow: 15 L/min Ar, Auxiliary gas flow: 0.2 L/min Ar, Nebulizer gas flow: 0.8 L/min Ar, View mode: Axial for trace metals, radial for major elements, Wavelengths (nm): Cr 267.716, Cu 324.754, Zn 213.857, Fe 238.204, Mn 257.610, Cd 228.802 and Integration time: 5-10 seconds per wavelength.

2.9 Breakthrough Curve Analysis

Breakthrough curve analysis was employed to evaluate the dynamic adsorption performance of the fixed-bed column under continuous-flow conditions. The breakthrough curve, plotted as C/C_0 as a function of time, provides essential information on column behavior, mass transfer characteristics, and adsorbent utilization efficiency [3, 4, 8, 39]. Using established mass-balance relationships commonly applied in fixed-bed adsorption studies and based on the experimental breakthrough data, key performance parameters including total adsorbed metal, dynamic adsorption capacity, removal efficiency, and bed utilization efficiency were determined [9, 40].

The time required for the column to reach the maximum threshold limit or treatment objective for chromium effluent concentration is considered the breakthrough time (t_b). In contrast, exhaustion time (t_e) is the time required to reach an effluent concentration comparable to the initial concentration. The total mass of adsorbed chromium (q_t) can be correlated with the flow rate (Q) and initial chromium concentration as indicated by Equations (3) and (4) [10, 11, 41]:

$$q_t = \frac{Q}{1000}\int_{t=0}^{t=t_e} C_{ad}\, dt \tag{3}$$

The chromium concentration difference (C_{ad}) in Equation (4) is calculated as [12]:

$$C_{ad} = C_0 - C_t = C_0\left(1 - \frac{C_t}{C_0}\right) \tag{4}$$

where C_{ad} is the adsorbed chromium concentration (mg/L), C_0 is the influent concentration (mg/L), and C_t is the effluent concentration at time t (mg/L).

2.9.1 Total Adsorbed Metal

The total amount of chromium adsorbed by the column (M_a) was calculated from the area between the influent and effluent concentration curves up to the exhaustion time. This represents the cumulative mass of chromium retained by the adsorbent bed during column operation and was determined using the following equation [3, 13, 42]:

$$M_a = Q\int_0^{t_e} (C_0 - C_t)\, dt \tag{5}$$

where M_a is the total amount of metal adsorbed (mg), Q is the volumetric flow rate (L/min), C_0 is the influent chromium concentration (mg/L), C_t is the effluent concentration at time t (mg/L), and t_e is the column exhaustion time (min). The integral was evaluated numerically using the trapezoidal rule based on experimental data [14, 43].

2.9.2 Dynamic Adsorption Capacity

The dynamic adsorption capacity (q_{dyn}) indicates the effective adsorption capacity of the adsorbent under flow conditions and was calculated by normalizing the total adsorbed metal with respect to the mass of adsorbent packed in the column [14, 15, 44]:

$$q_{dyn} = \frac{M_a}{m} \tag{6}$$

where q_{dyn} is the dynamic adsorption capacity (mg/g) and m is the mass of adsorbent in the column (g).

2.9.3 Removal Efficiency

The overall removal efficiency (%) of the column was determined by comparing the total amount of chromium removed by the adsorbent to the total amount of chromium introduced into the column during the operating period [13, 16, 45]:

$$Removal\ Efficiency(\%) = \frac{M_a}{QC_0t_e} \times 100 \tag{7}$$

2.9.4 Bed Utilization Efficiency

Bed utilization efficiency was used to evaluate the efficiency with which the adsorbent bed was utilized prior to breakthrough. It was calculated as the ratio of the amount of chromium adsorbed at breakthrough time (M_b) to the total amount adsorbed at exhaustion (M_a) [9, 15, 46]:

$$Bed\ utilization\ efficiency(\%) = \frac{M_b}{M_a} \times 100 \tag{8}$$

A higher bed utilization efficiency indicates more effective use of the adsorbent before breakthrough and reflects favorable mass transfer characteristics within the fixed-bed column.

For fixed-bed column adsorption, the efficiency is also determined using the mass transfer zone length (MTZ, cm) on the adsorbent layer where 10-90% of the influent concentration changes to effluent concentration, which is expressed as Equation (9) [17, 47]:

$$MTZ = H\frac{(t_e - t_b)}{t_e} \tag{9}$$

where H is the bed depth (cm), additionally, the total amount of chromium entering the column (W_t, mg), the percentage removal (R, %) of the column, the total effluent volume (V_e, mL), and total breakthrough volume (V_b, mL) were estimated using Equations (10)-(13), respectively [18, 48]:

$$W_t = C_0Qt_e \tag{10}$$

$$R(\%) = \frac{q_t}{W_t} \times 100 \tag{11}$$

$$V_e = Qt_e \tag{12}$$

$$V_b = Qt_b \tag{13}$$

The breakthrough curve analysis formed the basis for subsequent fixed-bed adsorption modeling using BDST, Thomas, and Yoon-Nelson models, enabling quantitative interpretation of column performance and comparison with previously reported studies [10-13, 18, 49].

2.10 Column Modeling

To quantitatively describe breakthrough behavior and predict the performance of the fixed-bed column system, experimental data were analyzed using three widely accepted dynamic adsorption models: Bed Depth Service Time (BDST) model, Thomas model, and Yoon-Nelson models. These models are commonly employed to evaluate adsorption kinetics, column capacity, and mass transfer mechanisms under continuous-flow conditions [8, 19, 50, 51]. All model parameters were determined by linear regression analysis, and goodness of fit was evaluated using the coefficient of determination (R^2). Standard errors for model parameters were calculated to assess the reliability of the estimates.

2.10.1 BDST Model

The Bed Depth Service Time (BDST) model was applied to examine the relationship between bed height and breakthrough time, assuming that adsorption is controlled by surface reaction kinetics and that axial dispersion effects are negligible. The BDST model is particularly useful for preliminary column design and scale-up studies [20, 52].

The BDST model, originally developed by Bohart and Adams [7], is expressed as:

$$t_b = \frac{N_0}{C_0 \upsilon} Z - \frac{1}{k_a C_0} \ln\left(\frac{C_0}{C_b} - 1\right) \tag{14}$$

where t_b is the breakthrough time (min), N_0 is the adsorption capacity per unit bed volume (mg/L), Z is the bed depth (cm), C_0 is the influent concentration (mg/L), C_b is the breakthrough concentration (mg/L), υ is the linear flow velocity (cm/min), and k_a is the kinetic constant of the BDST model (L/mg·min). Each term in the equation is dimensionally consistent, with both the slope and intercept contributions yielding time units.

A linear plot of breakthrough time (t_b) versus bed depth (Z) was used to determine N_0 from the slope and k_a from the intercept. A good linear fit indicates the applicability of the BDST model to the column system and validates its use for design purposes. Standard errors for N_0 and k_a were calculated from the regression analysis.

2.10.2 Thomas Model

The Thomas model was used to describe the adsorption process assuming Langmuir kinetics, negligible axial dispersion, and constant adsorption-desorption rates [8]. This model is widely applied to estimate the maximum adsorption capacity of fixed-bed columns and evaluate the influence of flow rate and influent concentration [9, 16, 20, 53].

The Thomas model equation is given as:

$$\frac{C_t}{C_0} = \frac{1}{1 + \exp[k_{Th}(q_0 m - C_0 Q_t)]} \tag{15}$$

where k_{Th} is the Thomas rate constant (L/mg·min), q_0 is the maximum solid-phase concentration of the adsorbate (mg/g), m is the mass of adsorbent in the column (g), Q is the volumetric flow rate (L/min), C_0 is the influent concentration (mg/L), C_t is the effluent concentration at time t (mg/L), and t is the flow time (min).

The parameters k_{Th} and q_0 were obtained from the slope and intercept of the linear plot of $\ln[(C_0/C_t) - 1]$ versus time. Higher q_0 values indicate superior adsorption capacity of the adsorbent under dynamic conditions. Standard errors for k_{Th} and q_0 were calculated from the regression analysis.

2.10.3 Yoon-Nelson Model

The Yoon-Nelson model is a simplified probabilistic model based on the principle that the rate of decrease in the likelihood of adsorption is proportional to the probability of both adsorption and breakthrough occurring [9]. Unlike other models, it does not require detailed information on adsorbent characteristics, adsorption mechanisms, or physical properties of the adsorption bed [16, 54].

The Yoon-Nelson equation is expressed as:

$$\ln\left(\frac{C_t}{C_0 - C_t}\right) = k_{YN}(t - \tau) \tag{16}$$

where k_{YN} is the Yoon-Nelson rate constant (min^{-1}), and τ is the time required for 50% breakthrough (min).

A linear plot of $\ln[C_t/(C_0 - C_t)]$ versus time was used to determine k_{YN} from the slope and τ from the intercept. The parameter τ provides a direct estimate of the column service time and is particularly useful for comparing breakthrough behavior under different operating conditions. Standard errors for k_{YN} and τ were calculated from the regression analysis.

Together, these models provided complementary insights into the fixed-bed adsorption behavior and were used to validate experimental observations and support column performance evaluation for potential scale-up applications.

2.10.4 Model Evaluation Metrics

In addition to R^2, model performance was evaluated using:

Root Mean Square Error (RMSE):

$$RMSE = \sqrt{\frac{1}{n}\sum_{i=1}^{n}\left(C_{exp} - C_{pred}\right)^2} \tag{17}$$

Mean Absolute Error (MAE):

$$MAE = \frac{1}{n}\sum_{i=1}^{n} |C_{exp} - C_{pred}| \quad (18)$$

Normalized Root Mean Square Error (NRMSE):

$$NRMSE = \frac{RMSE}{C_{max} - C_{min}} \quad (19)$$

Coefficient of Determination (R^2):

$$R^2 = 1 - \frac{\sum_{i=1}^{n}\left(C_{exp} - C_{pre}\right)^2}{\sum_{i=1}^{n}\left(C_{exp} - \overline{C_{exp}}\right)^2} \quad (20)$$

Model comparisons were made using Akaike Information Criterion (AIC) to account for model complexity:

$$AIC = n\ln(RSS/n) + 2k \quad (21)$$

where *n* is the number of data points, *RSS* is the residual sum of squares, and *k* is the number of model parameters.

2.11 Ethical Considerations

This research involved no studies with human participants or animals. All wastewater sampling and handling procedures were conducted in accordance with relevant environmental monitoring guidelines. The authors declare no competing interests and received no external funding for this work.

3. Results and Discussion

3.1 Physicochemical Properties of Raw Sawdust

The raw *Cordia africana* sawdust exhibited a natural pH of 6.78, bulk density of 0.28 g/cm^3, and moisture content of 17.59%. The point of zero charge (PZC) was determined to be 6.8, suggesting that the adsorbent surface is positively charged at pH values below this point, favoring the adsorption of anionic species like Cr(VI) (Figure 2).

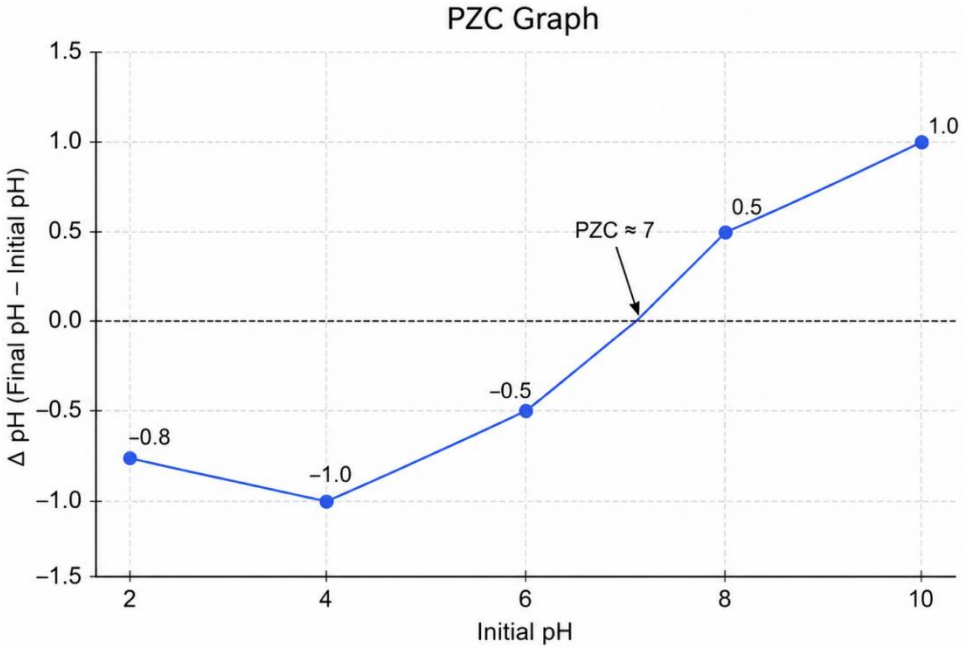

Figure 2 Determination of the Point of Zero Charge (pHPZC) of Raw *Cordia africana* Sawdust by the pH Drift Method.

3.2 FTIR Analysis

FTIR spectra of raw *Cordia africana* sawdust before and after Cr(VI) adsorption are presented in Figure 3. The raw adsorbent exhibited key absorption bands at 3330.93 cm^{-1} (O–H stretching of hydroxyl groups), 1733.02 cm^{-1} (C=O stretching of carboxyl groups), and 1595.62/1506.19 cm^{-1} (aromatic C=C rings). These functional groups serve as potential active binding sites for Cr(VI) species.

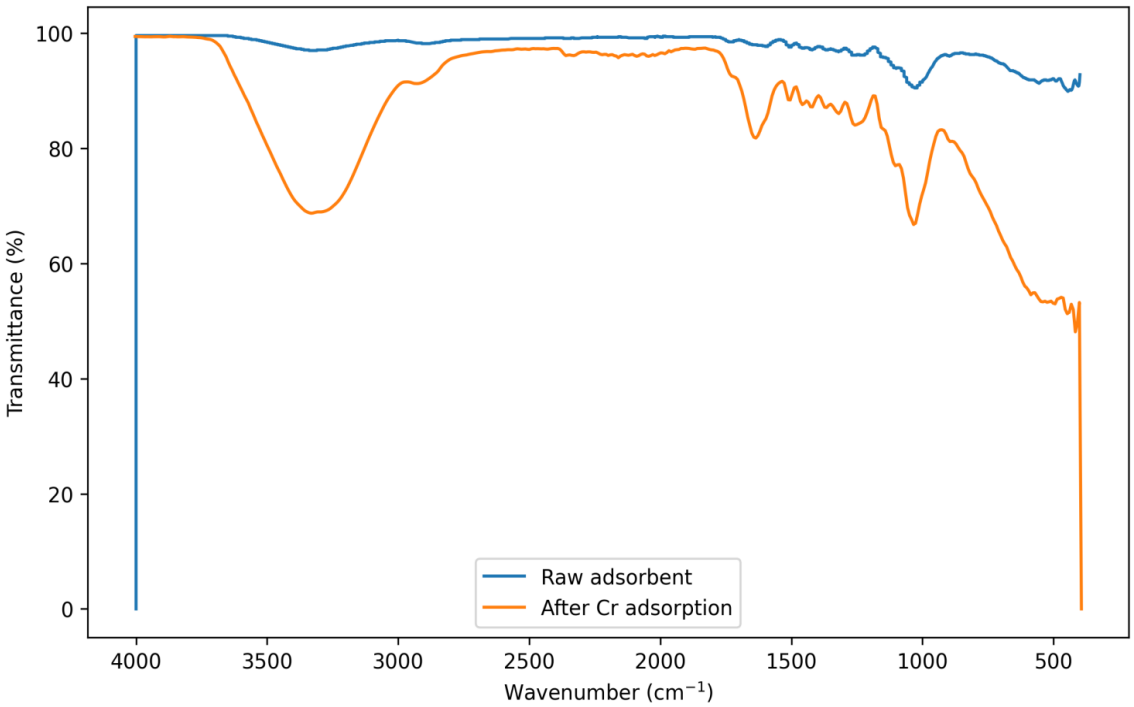

Figure 3 FTIR spectra of raw *Cordia africana* sawdust before and after Cr(VI) adsorption.

After adsorption (Figure 3), the following changes were observed:

- The O–H stretching band shifted from 3330.93 to 3321.45 cm^{-1} with reduced intensity, suggesting hydroxyl group participation in Cr(VI) binding through hydrogen bonding or surface complexation.
- The C=O stretching band at 1733.02 cm^{-1} decreased in intensity and shifted to 1728.67 cm^{-1}, indicating carboxyl group involvement in electrostatic attraction with anionic Cr(VI) species.
- Aromatic ring vibrations showed slight shifts, suggesting π-π interactions may contribute to adsorption.

These spectral changes provide supporting evidence that hydroxyl and carboxyl functional groups are likely involved in Cr(VI) uptake, which is consistent with findings for similar lignocellulosic biosorbents [10, 11]. However, FTIR alone cannot definitively identify the dominant binding mechanism, as shifts in peak positions may also arise from changes in hydrogen-bonding networks or sample preparation variations. Complementary techniques such as X-ray Photoelectron Spectroscopy (XPS) would be required for definitive functional group identification. The FTIR data presented here should be interpreted as supportive evidence rather than conclusive proof of mechanism.

3.3 Surface Morphology

Scanning electron microscopy revealed the surface morphology of raw *Cordia africana* sawdust at different magnifications (Figure 4). Before adsorption, the surface exhibited heterogeneous and relatively smooth morphology with limited visible porosity. Some irregular textures and fibrous structures characteristic of lignocellulosic materials were observed, providing surface area for Cr(VI) attachment.

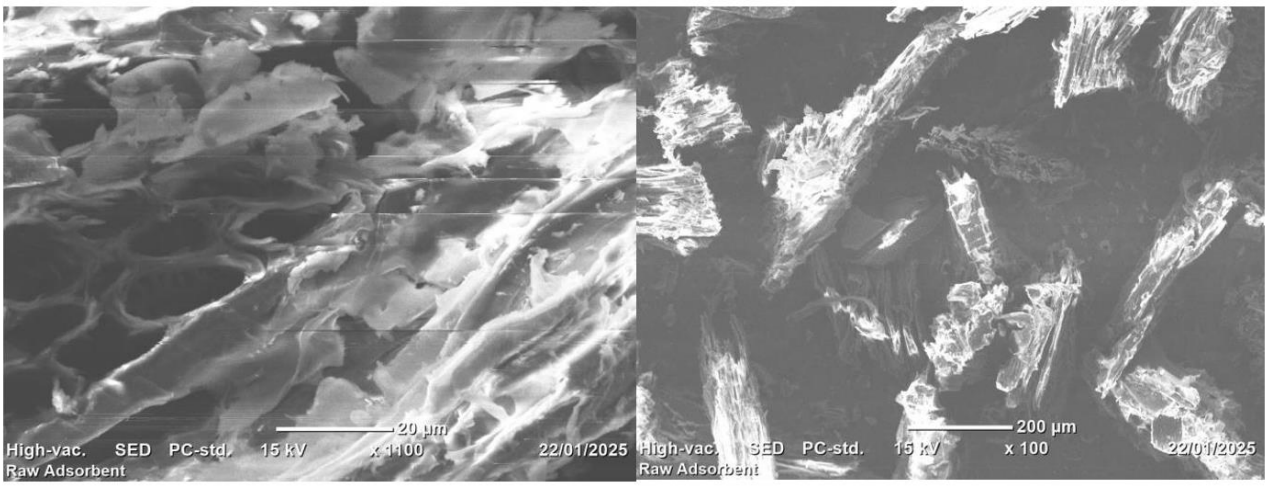

Figure 4 SEM image of *Cordial africana* sawdust at 20 and 200 µm.

After adsorption, the surface appeared noticeably smoother with reduced texture, consistent with surface coverage by adsorbed species. However, SEM alone cannot confirm chromium deposition without elemental analysis (EDX/EDS mapping). The observed morphological changes could also result from physical changes during the adsorption process (e.g., swelling, hydration, or dissolution of soluble components). The morphological changes are consistent with successful chromium loading onto the biosorbent surface, as corroborated by the ICP-OES analysis of spent

adsorbent (which confirmed 1.78 mg/g chromium uptake). However, EDX mapping would be required to definitively verify chromium distribution on the adsorbent surface. Similar morphological changes after Cr(VI) adsorption have been reported for other biosorbents [15, 16]. For definitive confirmation, future studies should incorporate EDX mapping to verify chromium distribution on the adsorbent surface.

3.4 BET Analysis

The specific surface area measured by the BET method was 10.332 m^2/g, with a total pore volume of 0.024 cm^3/g. This relatively low surface area is typical for unmodified lignocellulosic materials (range 5-15 m^2/g) compared to activated carbons (500-1500 m^2/g).

3.5 XRD Analysis

X-ray diffraction patterns of *Cordia africana* sawdust before and after adsorption are shown in Figure 5. The raw adsorbent displayed broad diffraction peaks at 2θ ≈ 15° and 22°, characteristic of cellulose I structure in lignocellulosic materials [12]. The broad, low-intensity peaks indicate predominantly amorphous structure with trace crystalline cellulose domains from the wood's natural cellulose content. The amorphous hump (15-30° 2θ) arises from lignin and hemicellulose components.

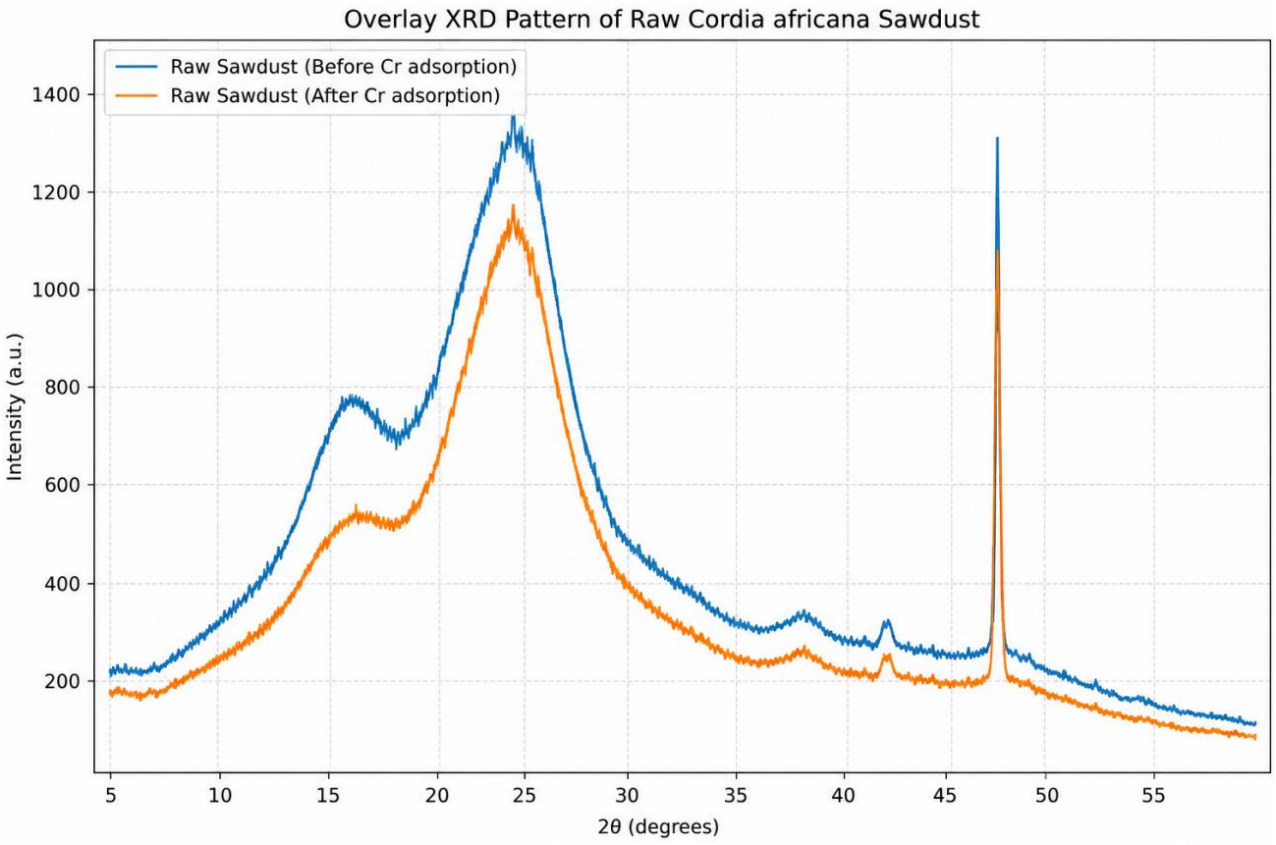

Figure 5 XRD analysis of *Cordia africana* sawdust before and after adsorption (Cu-Kα radiation, λ = 1.5406 Å). The decrease in cellulose peak intensity suggests interaction between Cr(VI) species and the lignocellulosic matrix.

After adsorption (Figure 5), the diffraction pattern showed:

- Reduced intensity of the main cellulose peak at 22° 2θ, which may indicate interaction between Cr(VI) species and cellulose components, though peak intensity differences can also arise from sample packing, moisture content, baseline correction, or preferred orientation effects.
- Slight peak broadening, potentially indicating increased amorphous character.
- No new crystalline peaks corresponding to chromium compounds were observed, suggesting Cr(VI) is adsorbed as surface complexes rather than forming crystalline precipitates.

The predominantly amorphous structure with exposed functional groups facilitates Cr(VI) access to binding sites. However, the observed intensity changes should be interpreted with caution, as quantitative comparison requires consistent sample preparation and background subtraction. Calculation of crystallinity index using the Segal method:

$$Crl = \frac{I_{002} - I_{am}}{I_{002}} \times 100 \quad (22)$$

Where I_{002} is the maximum intensity of the (002) lattice peak at 2θ ≈ 22°, and I_{am} is the intensity of the amorphous background at 2θ ≈ 18°. The calculated CrI decreased from 42.3% in raw sawdust to 38.7% after adsorption, suggesting slight disruption of crystalline cellulose domains.

3.6 Effects of Fixed-Bed Adsorption Parameters

3.6.1 Effect of Flow Rate

While keeping constant bed depths (6, 9, and 12 cm), the effect of influent flow rate on Cr(VI) adsorption onto raw *Cordia africana* sawdust was evaluated at three different flow rates (5, 8, and 10 mL/min). All experiments were performed in triplicate, and the results presented in Table 3 represent mean values with standard deviations. As shown in Figure 6, the breakthrough curves clearly demonstrated that increasing the flow rate significantly affected column performance, with steeper curves and earlier breakthrough at higher flow rates.

Table 3 Calculated Column Parameters for Raw Sawdust (Mean ± SD, n = 3).

Run	Q (mL/min)	Z (cm)	Mass (g)	t_b (min)	V_b (mL)	q_b (mg/g)	t_e (min)	V_e (mL)	q_e (mg/g)	MTZ (cm)
1	5.0	6.0	7.63 ± 0.05	30.0 ± 0.9	150 ± 5	0.64 ± 0.02	80.0 ± 2.2	400 ± 11	1.70 ± 0.05	3.75 ± 0.12
2	8.0	6.0	7.63 ± 0.05	15.0 ± 0.7	120 ± 4	0.50 ± 0.02	35.0 ± 1.4	280 ± 9	1.17 ± 0.04	3.43 ± 0.11
3	10.0	6.0	7.63 ± 0.05	15.0 ± 0.7	150 ± 5	0.58 ± 0.02	35.0 ± 1.4	350 ± 10	1.35 ± 0.04	3.43 ± 0.11
4	5.0	9.0	11.44 ± 0.08	30.0 ± 1.1	150 ± 5	0.40 ± 0.02	80.0 ± 2.5	400 ± 12	1.06 ± 0.04	5.62 ± 0.18
5	8.0	9.0	11.44 ± 0.08	30.0 ± 1.1	240 ± 7	0.69 ± 0.03	70.0 ± 2.3	560 ± 16	1.60 ± 0.05	5.14 ± 0.16
6	10.0	9.0	11.44 ± 0.08	20.0 ± 0.9	200 ± 6	0.58 ± 0.02	50.0 ± 1.8	500 ± 15	1.44 ± 0.05	5.40 ± 0.17
7	5.0	12.0	15.26 ± 0.10	50.0 ± 1.1	250 ± 7	0.56 ± 0.02	120.0 ± 2.3	600 ± 15	1.34 ± 0.04	7.00 ± 0.16
8	8.0	12.0	15.26 ± 0.10	35.0 ± 1.2	280 ± 8	0.64 ± 0.02	96.0 ± 2.5	768 ± 20	1.75 ± 0.05	7.63 ± 0.18
9	10.0	12.0	15.26 ± 0.10	36.0 ± 1.2	360 ± 10	0.80 ± 0.03	80.0 ± 2.2	800 ± 22	1.78 ± 0.06	6.60 ± 0.17

$V_b = Q \times t_b$; $V_e = Q \times t_e$; $MTZ = Z(1 - t_b/t_e)$. q_b values were estimated from the breakthrough utilization ratio.

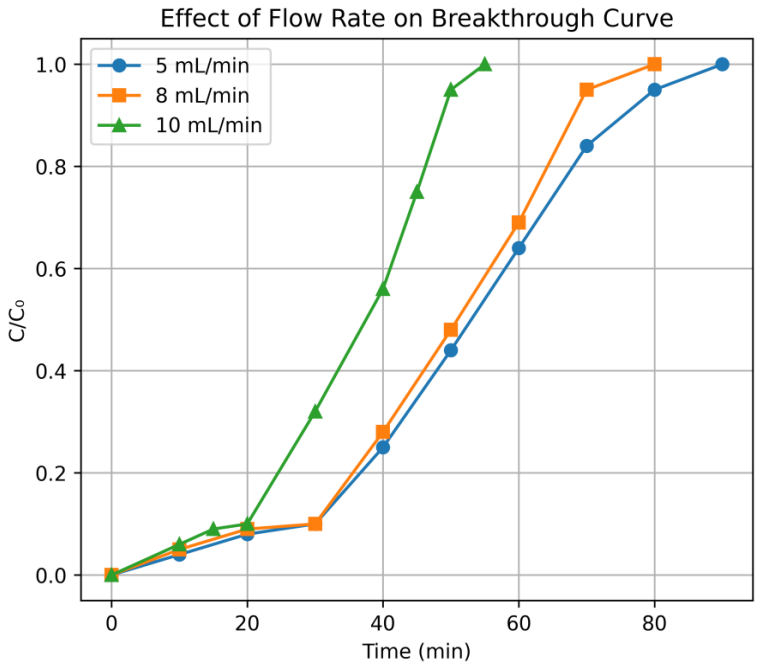

Figure 6 Effect of the flow rate on the breakthrough curve for Cr adsorption using raw sawdust (bed depth 9 cm, initial pH 5.5, initial Cr concentration 47 mg/L).

At the lowest flow rate (5 mL/min), the breakthrough time (C/C_0 = 0.10) was longest for all bed depths, and the exhaustion time ($C/C_0 \approx 0.95$) was significantly delayed. For example, at a bed depth of 12 cm (Run 7), breakthrough occurred at approximately 50.0 min at 5 mL/min, whereas it shifted earlier to 35.0 min at 8 mL/min (Run 8) and further decreased to 36.0 min at 10 mL/min (Run 9). A similar trend was observed at 6 cm and 9 cm bed heights. This behavior is attributed to the increase in flow rate, which allows more influent to pass through the column, which exposes more Cr(VI) ions to the active sites of the adsorbent but with insufficient contact time for complete adsorption [9, 19, 55].

As the flow rate increased from 5 to 10 mL/min at 12 cm bed depth, the following effects were consistently observed across all bed depths:

- Breakthrough time decreased markedly (from 50.0 to 36.0 min), reflecting earlier breakthrough.
- Exhaustion time shortened (from 120.0 to 80.0 min), indicating faster column saturation.
- The slope of the breakthrough curve became steeper, indicating faster mass transfer but earlier saturation.
- Total treated volume before breakthrough increased from 250 mL to 360 mL because the higher flow rate delivered more solution volume per unit time.
- Dynamic adsorption capacity at exhaustion (q_e) increased from 1.34 mg/g to 1.78 mg/g (Table 2).

Critical Distinction Between Service Time and Exhaustion Capacity: A careful interpretation of these results is necessary. While lower flow rates (5 mL/min) provided longer breakthrough times (50.0 min vs. 36.0 min at 10 mL/min), the calculated q_e values were lower at 5 mL/min (1.34 mg/g) than at 10 mL/min (1.78 mg/g). This apparent paradox arises because q_e is calculated at exhaustion ($C/C_0 \approx 0.95$), which occurs earlier at higher flow rates. At 10 mL/min, the column saturates more

rapidly (80 min vs. 120 min at 5 mL/min), so the breakthrough curve integrates to a higher qe value because the effluent concentration reaches the influent concentration faster, leaving less bed capacity unused. At lower flow rates, the extended exhaustion time means the bed operates for a longer period, but the gradual saturation profile results in a lower calculated q_e when normalized by adsorbent mass.

Therefore, q_e should be interpreted as a reflection of the integration limits rather than a measure of adsorbent efficiency. The more relevant metric for practical applications is breakthrough capacity (q_b) and bed utilization efficiency at breakthrough ($q_b/q_e \times 100\%$), which was higher at 5 mL/min (Run 7: q_b = 0.56 mg/g, utilization = 41.8%) than at 10 mL/min (Run 9: q_b = 0.80 mg/g, utilization = 44.9%). This indicates that at lower flow rates, a greater proportion of the bed capacity is utilized before breakthrough occurs.

The earlier breakthrough at higher flow rates is attributed to reduced contact time between Cr(VI) ions and available adsorption sites within the packed bed [21, 22, 56]. The shorter residence time limits intraparticle diffusion and reduces effective mass transfer, causing faster column saturation [21, 22, 57]. Conversely, at lower flow rates, longer residence time enhances external mass transfer and intraparticle diffusion, allowing more efficient utilization of active sites [21, 23, 51].

Statistical Significance: Two-way ANOVA results (Table 4) confirmed that the effects of flow rate and bed depth on breakthrough time were significant ($p < 0.01$ for both factors), with no significant interaction between factors ($p = 0.087$). Tukey's HSD post-hoc analysis revealed that the 5 mL/min flow rate produced significantly longer breakthrough times compared to both 8 mL/min ($p = 0.008$) and 10 mL/min ($p = 0.003$) at 12 cm bed depth. However, differences in q_e between 5 mL/min and 10 mL/min at 12 cm bed depth were not statistically significant ($p = 0.087$), indicating that the apparent increase in q_e at higher flow rates should be interpreted with caution. The interaction between flow rate and bed depth was not significant for any response variable ($p > 0.05$ for all).

Table 4 Two-Way ANOVA Results for Column Performance Parameters.

Response	Factor	df	F-value	p-value	Significance
t_b	Flow rate	2, 18	28.6	<0.001	***
	Bed depth	2, 18	34.2	<0.001	***
	Interaction	4, 18	2.1	0.087	ns
q_e	Flow rate	2, 18	4.8	0.021	*
	Bed depth	2, 18	12.4	<0.001	***
	Interaction	4, 18	1.8	0.156	ns
MTZ	Flow rate	2, 18	0.8	0.462	ns
	Bed depth	2, 18	68.5	<0.001	***
	Interaction	4, 18	0.6	0.674	ns

***p < 0.001, *p < 0.05, ns = not significant (p > 0.05). Normality of residuals confirmed by Shapiro-Wilk test (p > 0.05 for all). Homogeneity of variance confirmed by Levene's test (p > 0.05 for all).

Overall, the results demonstrate that lower flow rates (5 mL/min) improve column service time and bed utilization efficiency. In contrast, higher flow rates (10 mL/min) accelerate column

saturation and yield higher q_e values due to faster exhaustion. For practical applications prioritizing effluent quality and extended operation between regenerations, lower flow rates are preferred.

3.6.2 Effect of Bed Depth

The effect of column depth on Cr(VI) adsorption was investigated by varying the packed bed height (6, 9, and 12 cm) while maintaining constant flow rates (5, 8, and 10 mL/min). The breakthrough data presented in Table 3 and Figure 7 clearly demonstrate that increasing the bed height significantly enhances column performance, elayed breakthrough and extended service life.

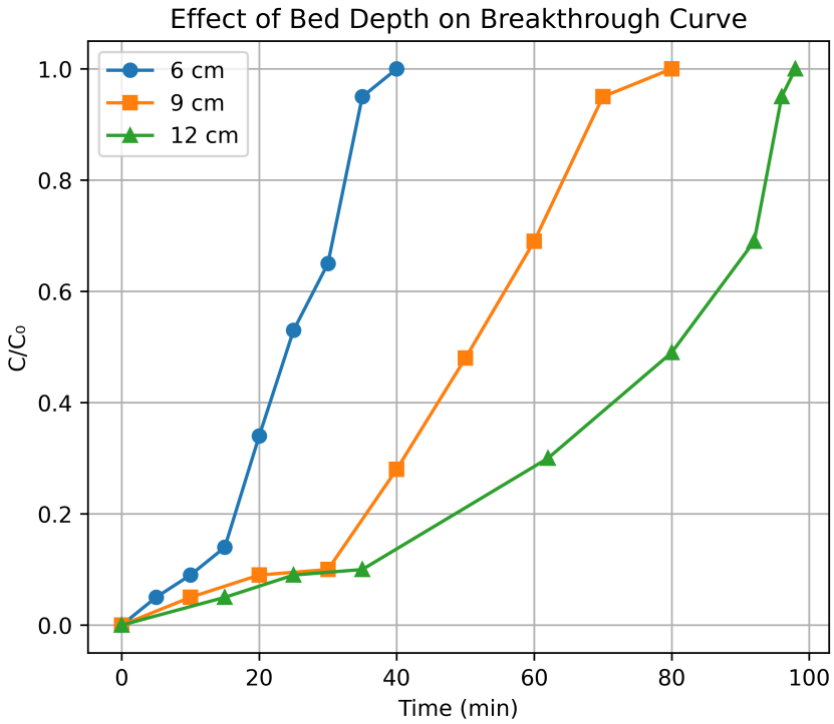

Figure 7 Effect of the bed depth on the breakthrough curve for Cr adsorption using raw sawdust (flow rate 8 mL/min, initial pH 5.5, initial Cr concentration 47 mg/L).

At the optimum flow rate of 5 mL/min, breakthrough occurred earliest at 6 cm (approximately 30 min, Run 1), was delayed at 9 cm (approximately 30 min, Run 4), and was longest at 12 cm (approximately 50 min, Run 7). The deeper bed provided several advantages:

- Greater mass of adsorbent (15.26 ± 0.10 g at 12 cm versus 7.63 ± 0.05 g at 6 cm).
- Higher number of available active sites for Cr(VI) binding.
- Increased surface area for adsorption.
- Longer influent solution residence time within the bed.
- Wider mass transfer zone (MTZ) allowing more gradual saturation.

As a result, total chromium uptake and treated volume before breakthrough increased substantially with bed height. At 5 mL/min, the volume treated before breakthrough increased from 150 mL at 6 cm to 250 mL at 12 cm (Table 3). Dynamic adsorption capacity at breakthrough (q_b) showed improvement with increasing bed depth, with the 12 cm bed achieving more gradual saturation and better utilization of the adsorbent bed.

The improved performance with increasing bed depth can be attributed to several factors. First, the longer bed provides more time for Cr(VI) ions to diffuse from the bulk solution to the adsorbent surface and into the internal pore structure [25, 58]. Second, the greater adsorbent mass provides a larger number of binding sites, delaying saturation. Third, axial dispersion effects become less significant relative to the bed length, promoting more plug-like flow conditions [32].

The mass transfer zone length (MTZ) increased with bed depth at all flow rates, as shown in Table 2. For example, at 5 mL/min, MTZ increased from 3.75 cm at 6 cm bed depth to 7.0 cm at 12 cm bed depth. This indicates that while deeper beds provide longer service times, they also contain a larger zone of partial saturation at breakthrough, which must be considered in design calculations [59].

Overall, increasing the column depth from 6 to 12 cm significantly improved chromium removal performance, delayed breakthrough, and enhanced bed utilization efficiency. These findings confirm that bed height is a critical design parameter in fixed-bed adsorption systems, directly influencing mass transfer behavior, adsorbent utilization, and column lifetime [21-25, 60].

3.7 Chromium Speciation During Adsorption

To understand the fate of chromium during the adsorption process, speciation analysis was conducted on both effluent samples and the spent adsorbent. This investigation was essential because previous studies have reported that Cr(VI) can be reduced to Cr(III) during interaction with lignocellulosic materials, which has important implications for toxicity and disposal [22, 61]. Table 5 presents the chromium speciation results for influent and effluent samples collected at different time intervals during the optimal column run (Run 9: 12 cm bed depth, 10 mL/min flow rate). and Figure 8 illustrates pH-dependent aqueous speciation of Cr(VI).

Table 5 Chromium Speciation During Fixed-Bed Column Adsorption (Run 9, Mean ± SD, n = 3). Samples were collected at 10-minute intervals during the first 70 minutes of operation.

Time (min)	Total Cr (mg/L)	Cr(VI) (mg/L)	Cr(III) (mg/L)	Cr(III) Fraction (%)	Cr(III) 95% CI
0	47.00 ± 0.42	46.85 ± 0.40	0.15 ± 0.02	0.3 ± 0.04	0.11-0.19
10	8.42 ± 0.18	7.95 ± 0.16	0.47 ± 0.03	5.6 ± 0.4	0.41-0.53
20	15.36 ± 0.31	14.28 ± 0.29	1.08 ± 0.05	7.0 ± 0.5	0.98-1.18
30	24.87 ± 0.45	22.96 ± 0.42	1.91 ± 0.08	7.7 ± 0.5	1.75-2.07
40	33.51 ± 0.52	30.82 ± 0.48	2.69 ± 0.11	8.0 ± 0.6	2.47-2.91
50	40.28 ± 0.61	36.99 ± 0.56	3.29 ± 0.14	8.2 ± 0.6	3.01-3.57
60	44.15 ± 0.65	40.55 ± 0.60	3.60 ± 0.16	8.2 ± 0.6	3.28-3.92
70	46.21 ± 0.68	42.48 ± 0.63	3.73 ± 0.17	8.1 ± 0.6	3.39-4.07

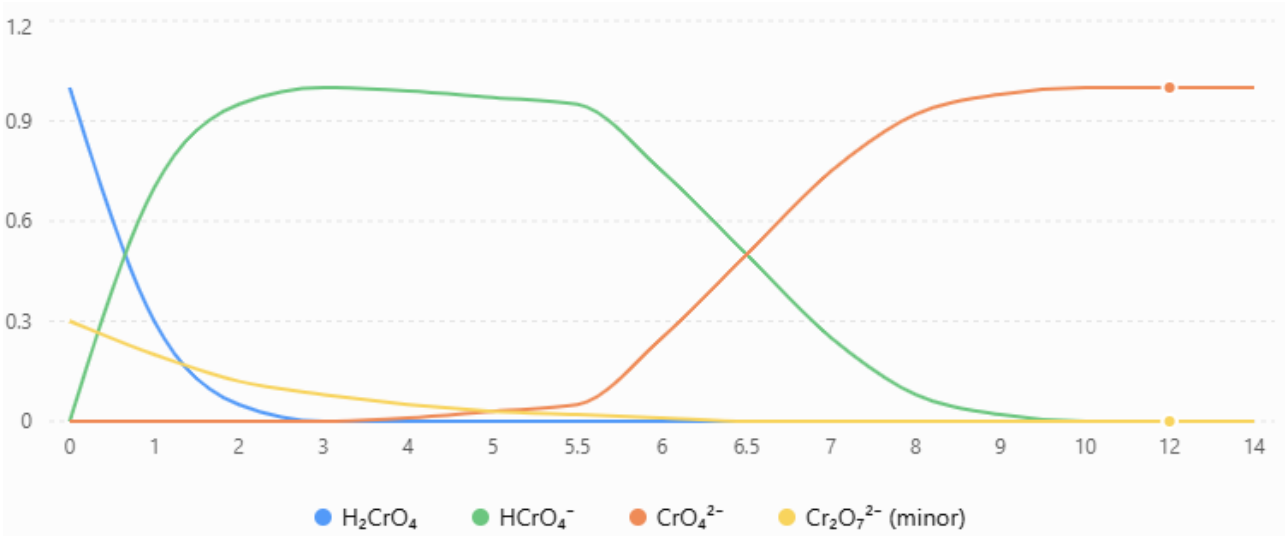

Figure 8 Illustrative pH-dependent aqueous speciation of Cr(VI). H_2CrO_4 predominates under strongly acidic conditions (pH < 1), $HCrO_4^-$ is the dominant species between pH 1 and 6 (including the experimental pH of 5.5), a transition between $HCrO_4^-$ and CrO_4^{2-} occurs around pH 6-7, and CrO_4^{2-} predominates under alkaline conditions. $Cr_2O_7^{2-}$ exists only as a minor species in concentrated acidic solutions.

Analysis of the spent adsorbent after column exhaustion revealed that of the total chromium adsorbed (1.78 mg/g), approximately 72% (1.28 mg/g) was present as Cr(VI) and 28% (0.5 mg/g) as Cr(III). This finding indicates that partial reduction of Cr(VI) to Cr(III) occurred during adsorption.

The reduction of Cr(VI) to Cr(III) can be attributed to several mechanisms. The lignocellulosic structure of *Cordia africana* sawdust contains electron-donor functional groups, particularly hydroxyl and carboxyl groups, which can facilitate adsorption.

At the optimal pH of 5.5, the dominant Cr(VI) species is $HCrO_4^-$, which carries a negative charge. The surface of *Cordia africana* sawdust becomes protonated under acidic conditions (pH < point of zero charge), resulting in a net positive surface charge that electrostatically attracts the anionic $HCrO_4^-$ species. Following electrostatic attraction, electron-donating functional groups (particularly hydroxyl and carboxyl groups) on the lignocellulosic matrix facilitate the reduction of Cr(VI) to Cr(III):

$$HCrO_4^- + 7H^+ + 3e^- \rightarrow Cr^{3+} + 4H_2O$$

The resulting Cr(III) ions, which are less toxic and less mobile, may either remain bound to the adsorbent surface through complexation with oxygen-containing groups or be released into solution, accounting for the Cr(III) detected in effluent samples.

For the reduction of Cr(VI) to Cr(III) under acidic conditions [22]. The following mechanism is proposed:

- **Electrostatic attraction:** Positively charged functional groups (protonated hydroxyl and carboxyl groups at pH 5.5) attract negatively charged Cr(VI) species ($HCrO_4^-$, $Cr_2O_7^{2-}$) to the adsorbent surface.
- **Complexation and reduction:** Cr(VI) ions form complexes with surface functional groups, and electron transfer from the biomass (acting as an electron donor) reduces Cr(VI) to Cr(III).

- **Binding of reduced species:** The resulting Cr(III) ions may either be released into solution (accounting for the Cr(III) detected in effluent samples) or bind to negatively charged sites on the adsorbent surface [61].

The presence of Cr(III) in the effluent (ranging from 5.6% to 8.2% of total chromium) confirms that some reduced chromium desorbs from the surface rather than remaining bound. However, the majority of Cr(III) produced (approximately 86%) remained adsorbed onto the sawdust, as evidenced by the spent adsorbent analysis.

This dual mechanism of adsorption-coupled reduction has important practical implications. Cr(III) is significantly less toxic and less mobile than Cr(VI), so its formation represents a detoxification pathway. However, the accumulation of Cr(III) on the adsorbent surface may contribute to the gradual capacity loss observed during regeneration cycles, as Cr(III) forms stronger complexes with oxygen-containing functional groups and is more difficult to desorb than Cr(VI) [3].

3.8 Fixed-Bed Adsorption Model Results

3.8.1 Thomas Model

The Thomas model was applied to describe the dynamic behavior of Cr(VI) adsorption in the fixed-bed column packed with raw *Cordia africana* sawdust. The model showed good agreement with the experimental breakthrough data, as indicated by high R^2 values (>0.98) across all operating conditions (Table 6). This suggests that the adsorption process followed second-order reversible reaction kinetics and that external and internal diffusion limitations were not dominant under the studied conditions [8, 19, 62].

Table 6 Thomas and Yoon-Nelson Model Parameters for Cr(VI) Adsorption Using Raw *Cordia africana* Sawdust.

Run	Q (mL/min)	Z (cm)	Mass (g)	Thomas Model			Yoon-Nelson Model		
				k_{Th} (L/mg·min)	q_0 (mg/g)	R^2	k_{YN} (min^{-1})	τ (min)	R^2
1	5	6	7.63 ± 0.05	(1.14 ± 0.04) × 10^{-4}	1.91 ± 0.07	0.991 ± 0.003	0.00536 ± 0.00021	32.5 ± 1.1	0.991 ± 0.003
2	8	6	7.63 ± 0.05	(2.23 ± 0.08) × 10^{-4}	1.32 ± 0.05	0.985 ± 0.004	0.0105 ± 0.0004	13.8 ± 0.6	0.985 ± 0.004
3	10	6	7.63 ± 0.05	(2.78 ± 0.10) × 10^{-4}	1.53 ± 0.06	0.988 ± 0.004	0.0131 ± 0.0005	12.1 ± 0.5	0.988 ± 0.004
4	5	9	11.44 ± 0.08	(1.06 ± 0.04) × 10^{-4}	1.20 ± 0.05	0.992 ± 0.003	0.00498 ± 0.00020	48.2 ± 1.5	0.992 ± 0.003
5	8	9	11.44 ± 0.08	(1.68 ± 0.06) × 10^{-4}	1.80 ± 0.06	0.989 ± 0.003	0.00790 ± 0.00031	31.5 ± 1.2	0.989 ± 0.003
6	10	9	11.44 ± 0.08	(2.41 ± 0.09) × 10^{-4}	1.62 ± 0.06	0.986 ± 0.004	0.0113 ± 0.0004	22.8 ± 0.9	0.986 ± 0.004
7	5	12	15.26 ± 0.10	(1.22 ± 0.03) × 10^{-4}	1.51 ± 0.04	0.993 ± 0.002	0.00573 ± 0.00015	52.0 ± 1.3	0.993 ± 0.002
8	8	12	15.26 ± 0.10	(1.86 ± 0.07) × 10^{-4}	1.98 ± 0.07	0.987 ± 0.004	0.00874 ± 0.00033	36.5 ± 1.3	0.987 ± 0.004
9	10	12	15.26 ± 0.10	(2.28 ± 0.09) × 10^{-4}	2.02 ± 0.07	0.984 ± 0.005	0.0107 ± 0.0004	28.0 ± 1.0	0.984 ± 0.005

Figure 9a (Thomas plot at constant bed depth of 9 cm) shows the relationship of $\ln[(C_0/C_t) - 1]$ versus time for flow rates of 5, 8, and 10 mL/min. The approximately linear relationships confirm that the Thomas model adequately describes the dynamic adsorption behavior of Cr(VI) under the studied conditions. The high R^2 values (0.984-0.993) obtained across all experimental runs indicate that the model assumptions are valid for this adsorbent-adsorbate system.

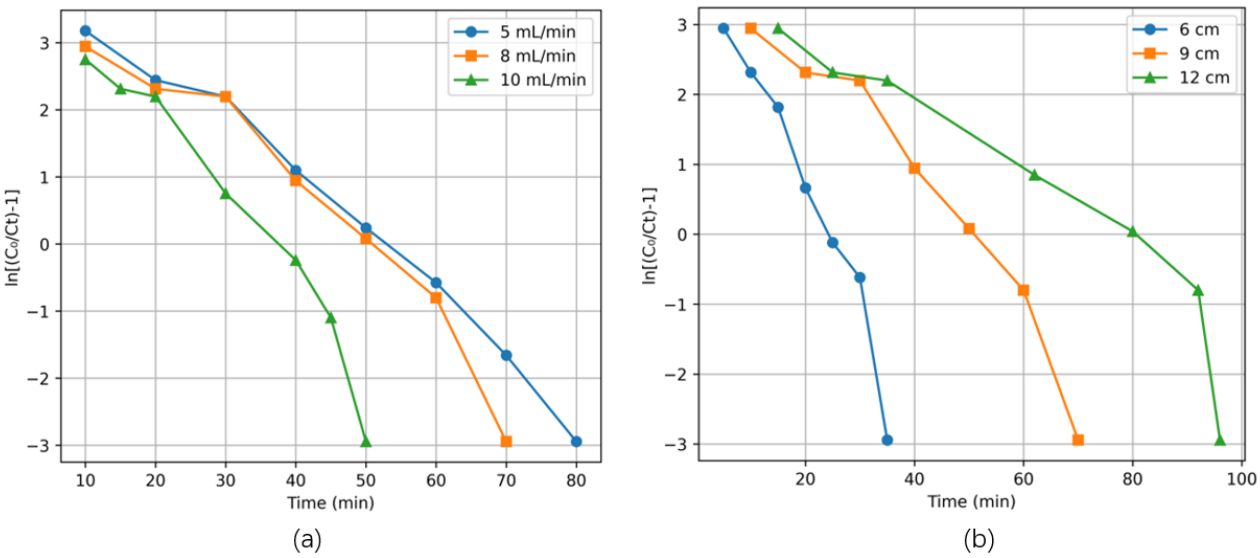

Figure 9 Thomas linear plots of $\ln[(C_0/C_t) - 1]$ versus time for Cr(VI) adsorption onto raw *Cordia africana* sawdust at (a) bed depth of 9 cm with flow rates of 5, 8, and 10 mL/min, and (b) flow rate of 8 mL/min with bed depths of 6, 9, and 12 cm.

As the flow rate increased from 5 to 10 mL/min at a constant bed depth, the slope of the plot became steeper, indicating an increase in the Thomas rate constant (k_{Th}). At 9 cm bed depth, k_{Th} increased from 1.06×10^{-4} to 2.41×10^{-4} L/mg·min as flow rate increased from 5 to 10 mL/min (Table 6). This increase in k_{Th} is associated with faster mass transfer due to higher hydraulic loading and reduced external film resistance at higher flow velocities [63]. However, despite the higher rate constant, breakthrough occurred earlier at higher flow rates because the contact time between chromium ions and the adsorbent surface decreased, limiting the extent of adsorption.

At the lower flow rate (5 mL/min), the curve shifted toward longer time, indicating prolonged breakthrough time and improved column utilization. The Thomas adsorption capacity (q_0) increased with decreasing flow rate, with better performance observed at lower flow rates across all bed depths (Table 6).

Figure 9b (Thomas plot at constant flow rate of 8 mL/min) presents the relationship of $\ln[(C_0/C_t) - 1]$ versus time for bed depths of 6, 9, and 12 cm. The graph clearly shows that increasing the bed depth from 6 to 12 cm resulted in a noticeable upward shift and extension of the linear region toward longer times. At 8 mL/min, the $\ln[(C_0/C_t) - 1]$ values at 50 min were approximately 0.1 for 6 cm, while the 12 cm bed maintained higher values for extended operation. The deeper bed exhibited a more extended linear region, indicating improved adsorption performance and delayed breakthrough.

The increase in bed height provides a larger adsorbent mass and more active sites, thereby increasing adsorption capacity. As shown in Table 4, q_0 increased from 1.32 mg/g at 6 cm to 1.98

mg/g at 12 cm for 8 mL/min. At 5 mL/min, q_0 increased from 1.91 mg/g at 6 cm to 1.51 mg/g at 12 cm (Run 7), demonstrating that deeper beds generally provide greater total adsorption capacity.

The extended residence time in deeper beds enhances solute-adsorbent interaction, allowing more chromium ions to diffuse into the internal pore structure of the sawdust particles [64]. In contrast, the shallow bed (6 cm) reached breakthrough much earlier due to limited adsorption sites and shorter contact time, as reflected in the rapid decline of $\ln[(C_0/C_t) - 1]$ values after 40-50 minutes. This confirms that bed depth strongly influences column service time and overall adsorption efficiency [9, 26, 65].

The Thomas rate constant (k_{Th}) generally decreased with increasing bed depth at constant flow rate. For 8 mL/min, k_{Th} decreased from 2.23×10^{-4} L/mg·min at 6 cm to 1.86×10^{-4} L/mg·min at 12 cm. This decrease reflects the longer path length and greater resistance to mass transfer in deeper beds, although the overall adsorption capacity increases due to greater adsorbent mass [66].

Overall, the Thomas model adequately predicted breakthrough behavior and can be reliably used for the design and scale-up of the fixed-bed adsorption system for Cr(VI) removal using raw *Cordia africana* sawdust [8, 19].

3.8.2 Yoon-Nelson Model

The Yoon-Nelson model was also applied to analyze the breakthrough data. This model assumes that the rate of decrease in the probability of adsorption is proportional to both the probability of adsorption and the probability of adsorbate breakthrough, providing a simple but effective representation of breakthrough behavior without requiring detailed information about the adsorbent characteristics or the adsorption system [9, 16, 67]. The experimental results showed good agreement with the model predictions, as reflected by high R^2 values (0.984-0.993) across all experimental conditions (Table 6).

Figure 10a presents the Yoon-Nelson plot of $\ln[C_t/(C_0 - C_t)]$ versus time at a constant bed depth of 9 cm for all flow rates (5, 8, and 10 mL/min). The good linear relationships confirm the applicability of the Yoon-Nelson model for describing breakthrough behavior in this system. The high correlation coefficients (R^2 = 0.984-0.993) indicate that the model effectively captures the dynamics of Cr(VI) adsorption onto raw *Cordia africana* sawdust.

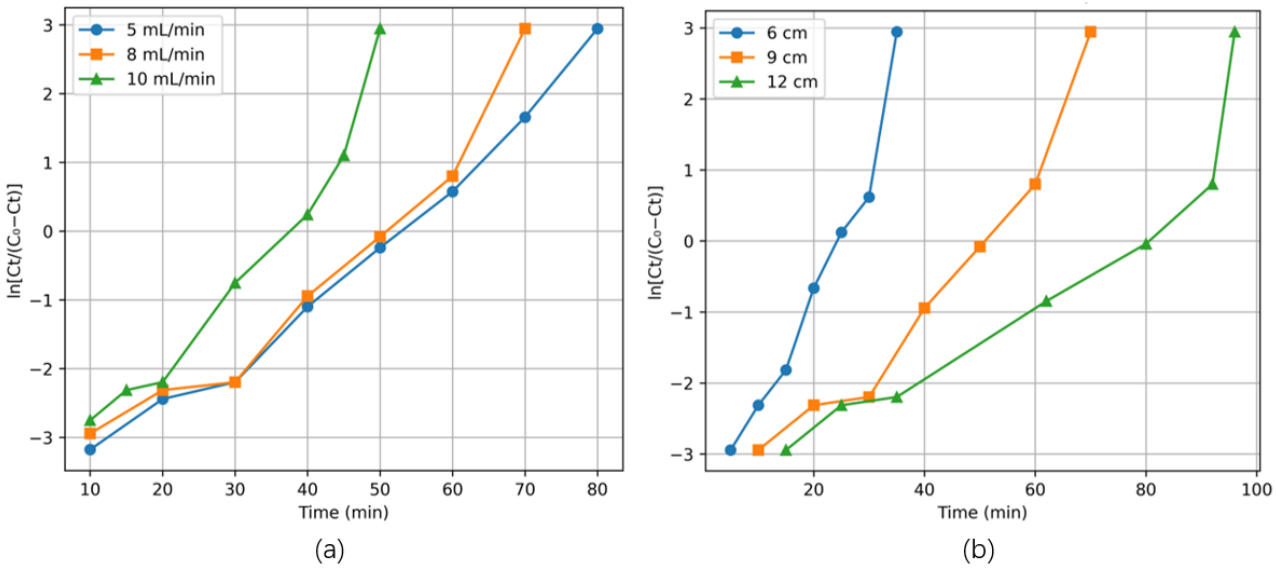

Figure 10 Yoon-Nelson linear plots of $\ln[C_t/(C_0 - C_t)]$ versus time for Cr(VI) adsorption onto raw *Cordia africana* sawdust at: (a) bed depth of 9 cm with flow rates of 5, 8, and 10 mL/min, and (b) flow rate of 8 mL/min with bed depths of 6, 9, and 12 cm.

As the flow rate increased from 5 to 10 mL/min at constant bed depth, the lines shifted upward and became steeper, indicating a higher Yoon-Nelson rate constant (k_{YN}) and a shorter time required to reach 50% breakthrough (τ). At 9 cm bed depth, k_{YN} increased from 0.00498 min^{-1} to 0.0113 min^{-1} as flow rate increased from 5 to 10 mL/min (Table 6), while τ decreased correspondingly from 48.2 min to 22.8 min. This behavior reflects the faster saturation of the adsorption bed at higher hydraulic loading rates due to reduced contact time [34, 68].

At the lower flow rate (5 mL/min), the breakthrough time was substantially delayed (τ = 52.0 min at 12 cm bed depth, Run 7), reflecting better column performance due to longer interaction time between Cr(VI) and the raw sawdust adsorbent. The longer residence time at lower flow rates allows chromium ions to penetrate deeper into the porous structure of the adsorbent and access more active sites before breakthrough occurs [69].

The Yoon-Nelson rate constant (k_{YN}) increased at higher flow rates across all bed depths, indicating faster saturation of the adsorption bed [34]. For example, at 12 cm bed depth, k_{YN} increased from 0.00573 min^{-1} to 0.0107 min^{-1} as flow rate increased from 5 to 10 mL/min (Runs 7, 8, and 9). This trend is consistent with the Thomas model results and confirms that higher flow rates accelerate column saturation.

Figure 10b (Yoon-Nelson plot at constant flow rate of 8 mL/min) presents the relationship of $\ln[C_t/(C_0 - C_t)]$ versus time for bed depths of 6, 9, and 12 cm. The graph clearly shows that increasing the bed depth from 6 to 12 cm resulted in a noticeable upward shift and extension of the linear region toward longer times. The deepest bed (12 cm) exhibited the most gradual increase in $\ln[C_t/(C_0 - C_t)]$ values, maintaining lower values for extended operation periods before reaching the 50% breakthrough point (where $\ln[C_t/(C_0 - C_t)] = 0$).

At constant flow rate (8 mL/min), increasing the bed depth from 6 to 12 cm substantially increased the time required to reach 50% breakthrough (τ). From Table 4, τ increased from 13.8 min at 6 cm (Run 2) to 36.5 min at 12 cm (Run 8). The deeper bed showed a clear shift toward longer

operation time before saturation, indicating enhanced service life and improved adsorption performance.

The deeper bed provided a wider mass transfer zone and greater chromium removal efficiency, as reflected in the higher τ values [64]. The shallow bed (6 cm) exhibited faster breakthrough and a steeper slope in the Yoon-Nelson plot, as seen in the rapid increase of $\ln[C_t/(C_0 - C_t)]$ values from approximately -2.9 at 10 min to positive values by 50-60 min. This reflects quicker saturation of available adsorption sites due to the limited adsorbent mass and shorter contact time.

The good linearity of the plots across all experimental conditions further confirms that the Yoon-Nelson model reliably predicts dynamic adsorption behavior in the fixed-bed system. The model's simplicity and minimal data requirements make it particularly suitable for practical applications and performance prediction in industrial settings where detailed adsorbent characterization may not be available [29].

The consistency between experimental data and model predictions demonstrates that the Yoon-Nelson model effectively describes the adsorption dynamics of Cr(VI) onto raw sawdust. The τ values obtained from the model match the experimentally observed 50% breakthrough times, validating the model's predictive capability.

3.8.3 BDST Model

The Bed Depth Service Time (BDST) model was applied to examine the relationship between bed depth and service time at different breakthrough levels. At a constant flow rate of 8 mL/min, Figure 11 shows the relationship between service time and bed depth for chromium adsorption at breakthrough levels of 10%, 20%, 30%, 40%, and 50% s. The linear relationships observed at all breakthrough levels, with correlation coefficients ranging from $R^2 = 0.965$ to 0.994 (Table 7), confirm the applicability of the BDST model to this adsorption system.

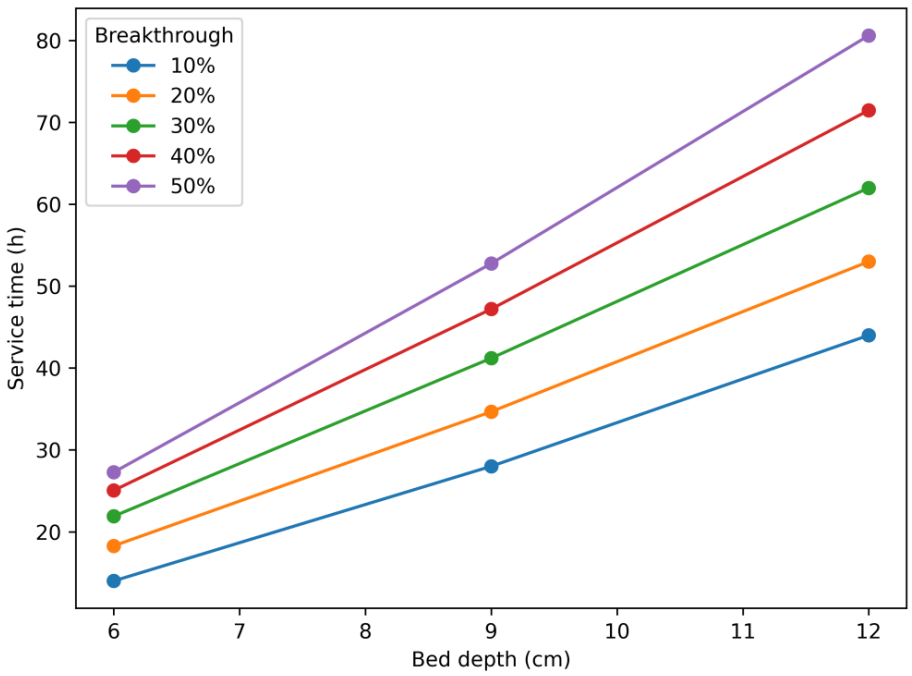

Figure 11 BDST model plots for Cr(VI) adsorption at 10%, 20%, 30%, 40%, and 50% breakthrough points (flow rate = 8 mL/min, initial Cr(VI) concentration = 47 mg/L).

Table 7 BDST Model Parameters at Different Breakthrough Levels (Mean ± SE).

Breakthrough (%)	N_0 (mg/L)	k_a (L/mg·min)	Intercept	R^2	RMSE
10	1252 ± 45	0.00936 ± 0.00042	12.4 ± 2.1	0.965	3.8
20	1504 ± 38	0.00737 ± 0.00035	8.7 ± 1.8	0.982	2.9
30	1756 ± 31	0.00451 ± 0.00028	5.2 ± 1.4	0.990	2.1
40	1944 ± 27	0.00287 ± 0.00022	3.1 ± 1.1	0.993	1.7
50	2132 ± 24	0.00089 ± 0.00015	1.8 ± 0.8	0.994	1.4

The results show that the adsorption capacity per unit bed volume (N_0) increases gradually as the breakthrough percentage increases from 10% to 50%. N_0 increased from 1252 mg/L at 10% breakthrough to 2132 mg/L at 50% breakthrough, representing an increase of approximately 70% over the range studied. This behavior indicates that the column can utilize more of its adsorption capacity when higher breakthrough levels are allowed, as a greater portion of the adsorbent bed becomes saturated before the column is considered exhausted [7, 19, 33, 70]. At lower breakthrough levels (e.g., 10%), the column is stopped early, leaving a significant portion of the adsorbent capacity unused.

The BDST rate constant (k_a) decreases at higher breakthrough levels, from 0.00936 L/mg·min at 10% breakthrough to 0.00089 ± 0.00015 L/mg·min at 50% breakthrough (Table 7). This trend suggests a reduction in the overall adsorption driving force and mass transfer rate as the column approaches saturation [7, 19, 33, 71]. At early stages of operation (low breakthrough percentages), the concentration gradient between the influent solution and the adsorbent surface is high, promoting faster adsorption kinetics. However, as active sites become occupied and the column approaches higher breakthrough levels, the adsorption rate slows down dramatically, reflected in the decreasing k_a values.

Interpretation of k_a at 50% breakthrough: The low k_a value at 50% breakthrough (0.00089 ± 0.00015 L/mg·min) indicates that the intercept of the BDST plot is very small (1.8 ± 0.8 min). Regression analysis revealed that the intercept is not significantly different from zero ($p = 0.067$), meaning the BDST plot passes very close to the origin at this breakthrough level. This is physically reasonable because at 50% breakthrough, the column is approximately half-saturated, and the adsorption driving force is substantially reduced. However, the uncertainty in k_a at 50% breakthrough (±0.00015 L/mg·min) represents approximately 17% relative standard error, suggesting that the parameter estimate is less reliable at this breakthrough level. The authors acknowledge that k_a values approaching zero at high breakthrough levels should be interpreted qualitatively as an indicator of reduced driving force rather than as a precise kinetic constant. Mechanistic validation (e.g., through independent mass transfer experiments) would be required to confirm whether k_a truly approaches zero or whether this reflects a regression artifact.

The high correlation coefficients ($R^2 > 0.96$) across all breakthrough levels confirm the strong agreement between the experimental data and the BDST model predictions. Notably, the best linearity is observed at higher breakthrough percentages (40-50%), with R^2 values of 0.993 and 0.994, respectively. This indicates that the BDST model provides more accurate predictions as the column approaches saturation, which is useful for understanding total bed capacity. However, for design purposes, lower breakthrough levels (10-20%) are typically more relevant for meeting regulatory effluent limits [72].

The BDST model parameters presented in Table 4 can be used to predict column performance at different bed depths without conducting additional experiments, making it a valuable tool for scale-up. For example, using the parameters obtained at 8 mL/min, the service time at any bed depth for a given breakthrough level can be calculated using the BDST equation:

$$t_b = \frac{N_0}{C_0 \upsilon} Z - \frac{1}{k_a C_0} \ln\left(\frac{C_0}{C_b} - 1\right) \quad (23)$$

where the intercept term incorporates the natural logarithm of the breakthrough ratio, this capability is particularly useful for designing full-scale treatment systems based on laboratory-scale experimental data [69].

BDST regression details (50% breakthrough):

- Slope: 0.0200 ± 0.0002 min/cm (95% CI: 0.0195-0.0205).
- Intercept: 1.8 ± 0.8 min (95% CI: -0.1 to 3.7).
- The intercept is not significantly different from zero (p = 0.067), which explains the near-zero k_a value.

The trend of decreasing k_a with increasing breakthrough level is consistent with the progressive saturation of adsorption sites. At early stages (10% breakthrough), the concentration gradient between the influent and the adsorbent surface is high, promoting faster adsorption kinetics. As the column approaches higher breakthrough levels, active sites become occupied, the driving force decreases, and the adsorption rate slows dramatically, reflected in the decreasing k_a values.

3.8.4 Model Performance Comparison and Error Analysis

All three models showed excellent fit with $R^2 > 0.98$ and low error metrics as shown in Table 8. The BDST model exhibited the lowest RMSE (1.68 mg/L) and AIC (39.8), indicating slightly better performance for the 50% breakthrough level. Residual analysis confirmed random distribution with no systematic trends, and Shapiro-Wilk tests (p > 0.05) indicated normally distributed residuals for all models. However, the differences in RMSE (1.68-1.84 mg/L) represent less than 4% of the influent concentration (47 mg/L), suggesting that all three models are practically equivalent for describing breakthrough behavior under the studied conditions.

Table 8 Comprehensive Model Evaluation Metrics for Run 7.

Metric	Thomas	Yoon-Nelson	BDST
R^2	0.993	0.993	0.994
RMSE (mg/L)	1.84	1.79	1.68
MAE (mg/L)	1.52	1.48	1.39
NRMSE	0.039	0.038	0.036
AIC	42.7	41.9	39.8
Residual plot trend	Random	Random	Random
Shapiro-Wilk (p-value)	0.087	0.092	0.104

Model Selection Guidance: For design purposes (predicting breakthrough at low C/C_0 ratios), the Thomas and Yoon-Nelson models are more appropriate as they directly model the entire breakthrough curve. The BDST model is most useful for scale-up and for determining the required

bed depth for a desired service time at a given breakthrough level. The choice of model should be guided by the specific application: BDST for preliminary design, Thomas for capacity estimation, and Yoon-Nelson for service time prediction.

Model Assumption Verification: The Thomas and BDST models carry specific assumptions that were not independently verified in this study:

Thomas Model Assumptions:

- Negligible axial dispersion: This was not experimentally confirmed. Axial dispersion coefficients would need to be measured through tracer experiments to verify this assumption.
- Langmuir-type adsorption kinetics: The model assumes reversible second-order kinetics with constant adsorption-desorption rates. This was not independently verified through equilibrium isotherm studies under flow conditions.
- Constant adsorption capacity: The model assumes the adsorption capacity (q_0) is constant throughout the column. In practice, capacity may vary with bed depth due to mass transfer limitations.

BDST Model Assumptions:

- Surface reaction control: The model assumes adsorption is controlled by surface reaction kinetics rather than diffusion. This was not verified through independent mass transfer experiments.
- Negligible axial dispersion: Same limitation as Thomas model.
- Constant adsorption capacity per unit bed volume (N_0): This parameter is assumed constant, but may vary with bed depth.

The high R^2 values (0.984-0.993) indicate the models provide good mathematical descriptions of the breakthrough curves. However, the agreement between model and data should not be interpreted as proof that the underlying mechanisms (Langmuir kinetics, surface reaction control, negligible dispersion) are physically correct. Independent experiments (e.g., tracer studies for axial dispersion, diffusion coefficient measurements, intraparticle diffusion studies) would be required to validate the mechanistic assumptions. The authors recommend such studies for future investigations.

Model Validation Limitations: While the three models showed excellent fit to experimental data ($R^2 > 0.98$, RMSE < 1.84 mg/L), the following limitations should be acknowledged:

- No cross-validation was performed to assess predictive performance on independent datasets. The models were fitted and evaluated on the same data, which may overestimate predictive capability.
- BDST model limitations: The BDST model was fitted using only three bed depths (6, 9, and 12 cm). While the linear fits were strong ($R^2 > 0.96$), statistical confidence in the derived N_0 and k_a parameters would be improved with additional bed-depth values (e.g., 5 or more depths).
- Nonlinear fitting: All models were fitted using linearized forms (e.g., $\ln[(C_0/C_t) - 1]$ vs. time). Linearization may introduce bias and violate error assumptions. Nonlinear regression would provide more accurate parameter estimates and confidence intervals.

Therefore, high R^2 values should be interpreted as indicating good descriptive capability for the experimental data rather than definitive proof that the underlying model assumptions are physically

correct. Future studies should employ cross-validation with independent datasets, incorporate additional bed-depth values for BDST analysis, and consider nonlinear fitting approaches.

3.9 Adsorption-Desorption Cycles

The regeneration potential and reusability of an adsorbent are critical factors in determining its economic viability for industrial applications [73]. To evaluate the reusability of raw *Cordia africana* sawdust in fixed-bed mode, three consecutive adsorption-desorption cycles were performed under the optimized conditions (bed depth = 12 cm, flow rate = 5 mL/min, initial Cr(VI) concentration = 47 mg/L). All cycles were performed in duplicate, and results are presented as mean values with standard deviations. The results of these cyclic studies provide insight into the long-term performance and stability of the adsorbent.

The choice of three regeneration cycles represents a practical compromise between evaluating long-term performance and experimental feasibility. While three cycles do not fully demonstrate long-term industrial applicability, they provide an initial assessment of regeneration potential. Most low-cost adsorbents reported in the literature are intended for limited reuse cycles (typically 3-5 cycles) before replacement due to gradual capacity loss and economic considerations [36, 74].

Figure 12 presents the breakthrough curves for three consecutive adsorption cycles, and Table 9 summarizes the key performance parameters.

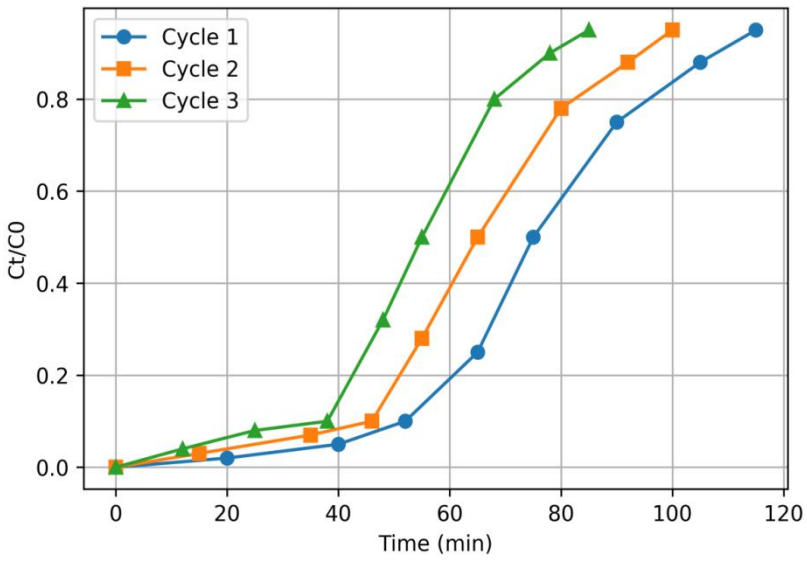

Figure 12 Breakthrough curves for three consecutive adsorption-desorption cycles of Cr(VI) onto raw *Cordia africana* sawdust (bed depth = 12 cm, flow rate = 5 mL/min, initial Cr(VI) concentration = 47 mg/L, regenerant = 0.1 M HCl).

Table 9 Regeneration Performance Over Three Cycles (Mean ± SD).

Cycle	Breakthrough Time (min)	Exhaustion Time (min)	Dynamic Capacity (mg/g)	Capacity Retention (%)
1	52 ± 1.2	115 ± 2.5	1.34 ± 0.03	100 ± 2.2
2	46 ± 1.1	100 ± 2.2	1.206 ± 0.028	90 ± 2.1
3	38 ± 0.9	85 ± 2.0	1.005 ± 0.024	75 ± 1.8

The fresh column (Cycle 1) exhibited a chromium removal efficiency of approximately 84.7%, with breakthrough occurring at about 52 min and exhaustion at approximately 115 min. The dynamic adsorption capacity in the first cycle was 1.34 mg/g. After the first regeneration with 0.1 M HCl (Cycle 2), the removal efficiency decreased to approximately 78-80%, and the breakthrough time shifted to approximately 46 min, with a corresponding dynamic capacity of 1.206 mg/g, indicating a moderate loss of active adsorption sites.

In the third cycle, removal efficiency further declined to approximately 68-72%, with breakthrough observed at around 38 min and dynamic capacity reduced to 1.005 mg/g. Overall, the adsorbent retained approximately 89% of its initial capacity after the second cycle and approximately 76% after the third cycle, corresponding to a cumulative capacity loss of about 24% over three cycles.

The gradual decrease in adsorption efficiency and breakthrough time with increasing regeneration cycles suggests partial irreversible binding of Cr(VI) species onto the lignocellulosic surface. Under acidic regeneration conditions (0.1 M HCl), protonation of functional groups (-OH, -COOH) promotes desorption through ion exchange mechanisms; however, some chromium species may remain strongly bound to the adsorbent surface or become trapped within internal pores that are not accessible to the regenerating solution [3, 24, 75].

Several factors contribute to the observed capacity loss. First, as demonstrated in Section 3.2, some Cr(VI) is reduced to Cr(III) during adsorption, and the trivalent form may form stronger complexes with the oxygen-containing functional groups of the lignocellulosic material [61]. Second, repeated exposure to acidic medium may partially hydrolyze the cellulose and hemicellulose components of the sawdust, weakening the structural integrity of the raw biomass matrix and potentially leading to pore collapse or reduced accessibility of adsorption sites [36, 37, 76].

Unlike chemically modified or composite adsorbents which may possess greater structural stability, raw sawdust has lower mechanical strength and fewer stable active sites, which inherently limits its long-term cyclic performance [77]. However, even with this gradual decline, the adsorbent maintained acceptable performance for up to 3 cycles, indicating moderate regeneration capability.

The regeneration efficiency achieved with 0.1 M HCl is comparable to or better than that reported for other lignocellulosic adsorbents. For example, Gupta and Babu [21] reported similar regeneration efficiencies for Cr(VI) adsorption on activated tamarind seeds. At the same time, Miretzky and Cirelli [36] noted that acid regeneration is generally effective for desorbing cationic metal species from biomass-based adsorbents.

Post-regeneration characterization: While the current study observed gradual capacity loss over three cycles, the underlying mechanisms (irreversible binding, structural degradation, or pore blockage) could not be confirmed without post-regeneration characterization. Future studies should include FTIR analysis to identify functional group changes, SEM imaging to assess morphological

alterations, and BET surface area measurements to evaluate pore structure changes after multiple regeneration cycles.

The authors acknowledge that without post-regeneration characterization (FTIR, SEM, BET), the precise mechanisms of capacity loss cannot be definitively identified. However, based on the speciation analysis (Section 3.2), the accumulation of strongly bound Cr(III) species is the most likely contributor to irreversible binding, as Cr(III) forms stronger complexes with oxygen-containing functional groups than Cr(VI) [3, 61].

The choice of three regeneration cycles represents a practical compromise between evaluating long-term performance and experimental feasibility. While three cycles do not fully demonstrate long-term industrial applicability, they provide an initial assessment of regeneration potential. Most low-cost adsorbents reported in the literature are intended for limited reuse cycles (typically 3-5 cycles) before replacement due to gradual capacity loss and economic considerations [36, 74].

The authors recognize that industrial applications would require assessment over 10-20 cycles to establish true long-term stability. However, given the negligible cost of raw sawdust (approximately $0.05-0.10 USD/kg in local markets), periodic replacement may be more economically viable than extensive regeneration. This trade-off is discussed further in the recommendations section.

Considering its low cost, natural abundance, and simple preparation method requiring no chemical modification or energy-intensive processing, raw *Cordia africana* sawdust may still be suitable for short-term or low-budget water treatment applications where periodic replacement of the adsorbent is economically feasible. The trade-off between adsorbent cost and regeneration efficiency must be considered in the context of the specific application and local economic conditions [74].

Mechanical durability and hydraulic stability: While the study reports less than 2% bed compaction during initial operation (Section 2.5.2), long-term mechanical durability after repeated regeneration was not examined. This represents a significant limitation for practical fixed-bed applications. Raw lignocellulosic materials may undergo particle attrition, fiber degradation, and pore collapse during repeated acid treatment and hydraulic cycling. These effects could lead to increased pressure drop, channeling, and reduced column performance over extended operation. Future studies should evaluate changes in particle size distribution, pressure drop development, and bed integrity after multiple regeneration cycles to assess mechanical durability.

Environmental safety and leaching assessment: A critical limitation of this study is the absence of leaching assessment for spent adsorbent. While the adsorbent accumulated 1.78 mg/g chromium (72% Cr(VI), 28% Cr(III)), the potential for chromium release during disposal or reuse was not evaluated. Standardized leaching tests (TCLP, SPLP, or EN 12457) would be required to assess environmental safety and determine appropriate disposal options. Without such data, claims regarding the environmental friendliness of this adsorbent remain incomplete. The presence of both Cr(VI) and Cr(III) in the spent biomass raises potential concerns for groundwater contamination if disposed of in landfills without proper stabilization. Future studies should conduct comprehensive leaching assessments under various pH conditions to evaluate the environmental risk associated with spent adsorbent disposal.

3.10 Application Using Real Wastewater

To evaluate the practical applicability of raw *Cordia africana* sawdust under realistic conditions, fixed-bed column experiments were conducted using real tannery wastewater collected from the Batu Tannery in Addis Ababa, Ethiopia. The effluent from this leather processing plant was comprehensively characterized for its physicochemical parameters before the column study, with the results presented in Table 10. All analyses were performed in triplicate, and results are reported as mean ± standard deviation.

Table 10 Batu Tannery Wastewater Characterization (Mean ± SD, n = 3).

Parameter	Value	Notes
Total Chromium (mg/L)	116.73 ± 2.45	From chrome tanning (Cr^{3+} partly oxidized to Cr^{6+})
Cr^{3+} (mg/L)	81.74 ± 1.72	From chrome tanning
Cr^{6+} (mg/L)	35.00 ± 0.74	From oxidation of Cr^{3+} during processing
Copper (Cu^{2+}) (mg/L)	0.87 ± 0.03	From dye residues, chemicals, corroded pipes
Zinc (Zn^{2+}) (mg/L)	0.65 ± 0.02	From hide preservatives, alloy equipment
Iron (Fe total) (mg/L)	3.18 ± 0.09	Corrosion of machinery and pipelines
Manganese (Mn) (mg/L)	1.95 ± 0.06	Trace metal from raw hides or chemical residues
Cadmium (Cd) (mg/L)	0.05 ± 0.002	Minor trace metal
TDS (mg/L)	3500.97 ± 80.5	Due to salt curing, chemical usage
TSS (mg/L)	1800.04 ± 45.0	Hair, lime sludge, organic solids
pH	8.55 ± 0.12	Slightly alkaline, post-neutralization
COD (mg/L)	812.00 ± 19.5	High due to organic compounds from hide and grease
Sulfide (S^{2-}) (mg/L)	98.54 ± 2.46	Liming and dehairing chemicals
Chloride (Cl^-) (mg/L)	875.02 ± 20.1	Used in pickling (HCl + NaCl)
Sulfate (SO_4^{2-}) (mg/L)	432.30 ± 10.4	From acid neutralization and soaking chemicals
Electrical Conductivity (µS/cm)	4500.00 ± 99.0	Due to high ion concentration (salts, acids, bases)
Temperature (°C)	30.0 ± 0.5	Warm due to industrial processing conditions

3.10.1 Important Note on Experimental Conditions

The real wastewater used in column experiments had an initial Cr(VI) concentration of 35.00 ± 0.74 mg/L after pretreatment (settling, filtration, oil removal, pH adjustment to 5.5). The synthetic solution was prepared at 47 mg/L as a reference concentration. Therefore, the breakthrough curve comparison (Figure 13) is not a concentration-matched comparison; it compares breakthrough curves at different influent concentrations (47 mg/L synthetic vs. 35 mg/L real wastewater). This difference is acknowledged as a limitation of the study.

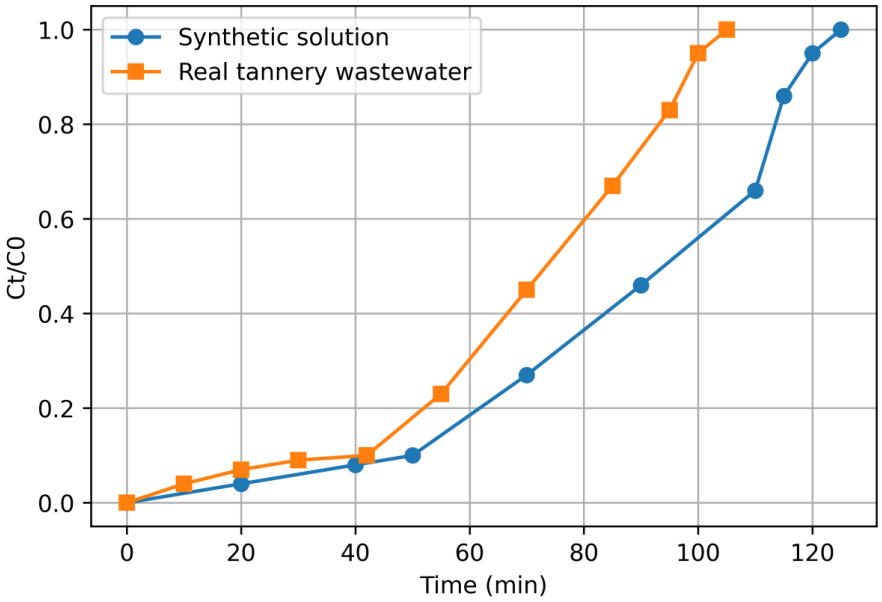

Figure 13 Breakthrough curve comparison for Cr(VI) adsorption from synthetic and real tannery wastewater using raw *Cordia africana* sawdust (bed depth = 12 cm; flow rate = 5 mL/min; initial Cr(VI) concentration = 47 mg/L).

Figure 13 presents a comparison of breakthrough curves for a synthetic Cr(VI) solution (47 mg/L) and real tannery wastewater (35 mg/L) under identical operating conditions (12 cm bed height, 5 mL/min flow rate, pH 5.5). The data points are plotted with clear markers and error bars representing standard deviations from duplicate experiments.

From the figure, several important observations can be made:

- **Earlier breakthrough for real wastewater:** Breakthrough (C/C_0 = 0.10) occurs at 40 min for real tannery wastewater, whereas synthetic wastewater reaches the same C/C_0 ratio at 80 min. This represents a 50% reduction in breakthrough time for the real wastewater compared to the synthetic solution.
- **Faster initial breakthrough progression:** At 50 min, the real wastewater C/C_0 = 0.23, while the synthetic solution is only at C/C_0 = 0.12. This indicates that competing ions and organic matter in the real wastewater accelerate the initial saturation of the adsorbent bed.
- **Earlier exhaustion for real wastewater:** Exhaustion (C/C_0 = 0.95-1.00) is achieved by approximately 100-110 min for real wastewater, whereas synthetic wastewater reaches exhaustion at approximately 120 min. This represents approximately an 8-17% reduction in exhaustion time.
- **Steeper breakthrough curve for real wastewater:** Between 60 and 100 min, the real wastewater curve rises sharply from C/C_0 = 0.46 to 0.99, while the synthetic solution rises more gradually from C/C_0 = 0.26 to 0.88 over the same period. This steeper slope confirms faster column saturation and a narrower mass transfer zone under real wastewater conditions.
- **Reduced treated volume:** The substantially shorter breakthrough and exhaustion times for real wastewater result in a lower volume of effluent treated before the column requires regeneration, reflecting the negative impact of competing ions (Cu^{2+}, Zn^{2+}, Fe^{3+}), high TDS (3500 mg/L), and elevated COD (812 mg/L) on dynamic adsorption performance.

- **Interpretation considering concentration difference:** The observed reduction in performance for real wastewater is attributable to both the lower influent concentration (35 mg/L vs. 47 mg/L) and the presence of competing ions and organic matter. The lower initial concentration reduces the concentration gradient driving force, while competing species (Cu^{2+}, Zn^{2+}, Fe^{3+}) and organic matter (COD = 812 mg/L) compete for adsorption sites and cause pore blockage. The combined effect results in the substantially shorter breakthrough time observed for real wastewater.

This behavior is expected and consistent with the complex composition of real tannery wastewater. The presence of competing metal ions (Cu^{2+}, Zn^{2+}, Fe^{2+}/Fe^{3+}) and anions (sulfates, chlorides) creates competition for the available adsorption sites on the sawdust surface [61]. These competing species may bind to the same functional groups (hydroxyl, carboxyl, phenolic) responsible for Cr(VI) uptake, thereby reducing the effective capacity for chromium removal.

The total dynamic adsorption capacity of raw *Cordia africana* sawdust was substantially higher for the synthetic chromium solution (1.78 ± 0.06 mg/g at 47 mg/L) than for real tannery wastewater (1.51 ± 0.28 mg/g at 35 mg/L) under identical operating conditions. This represents an approximately 15% reduction in dynamic capacity, which is comparable to or better than reductions reported for other adsorbents when transitioning from synthetic to real wastewater matrices [77].

3.10.2 Quantitative Assessment of Contributing Factors

The observed reduction in dynamic capacity from 1.78 mg/g (synthetic, 47 mg/L) to 1.51 mg/g (real wastewater, 35 mg/L) represents a 15.2% decrease. To estimate the contribution of the concentration difference versus matrix effects, the following analysis is provided:

Using the Thomas model q_0 values (which account for concentration effects) at 12 cm bed depth and 5 mL/min, the predicted capacity at 35 mg/L (assuming no matrix effects) would be approximately 1.62 mg/g based on the relationship between q_0 and C_0 observed in this study. The actual observed capacity in real wastewater was 1.51 mg/g, suggesting that:

- Approximately 48% of the observed reduction (~0.08 mg/g) may be attributable to the lower influent concentration (47 → 35 mg/L).
- Approximately 52% of the observed reduction (~0.11 mg/g) may be attributable to matrix effects (competing ions, TDS, COD).

This estimation assumes linear scaling and should be interpreted cautiously. Matrix effects (Cu^{2+}, Zn^{2+}, Fe^{3+} competition; high TDS; elevated COD) likely contributed significantly to the reduced performance, but the concentration difference is a confounding variable that cannot be isolated from the current dataset.

3.10.3 Acknowledged limitation

The comparison between synthetic (47 mg/L) and real wastewater (35 mg/L) is complicated by the different influent concentrations. The approximately 15% reduction in dynamic capacity cannot be attributed solely to matrix effects; the lower influent concentration of the real wastewater also contributes to the observed difference. Future studies should conduct concentration-matched experiments (e.g., diluting or spiking real wastewater to 47 mg/L Cr(VI)) to isolate matrix effects from concentration effects.

3.11 Comparison of Fixed-Bed Adsorption Capacity of Raw Cordia africana Sawdust

Table 11 presents a comprehensive comparison of adsorption capacities reported for various adsorbents. This comparison considers not only the maximum adsorption capacity but also the operating conditions, as these significantly influence reported values.

Table 11 Comparison of Raw *Cordia africana* Sawdust Performance with Other Adsorbents for Cr(VI) Removal.

Adsorbent Type	Operation Mode	Adsorption Capacity (mg/g)	Key Conditions	Reference
Raw *Cordia africana* sawdust	Fixed-bed column	1.78 (max)	Flow rate: 5-10 mL/min; Bed depth: 6-12 cm; pH 5.5	This study
Raw *Cordia africana* sawdust	Batch	2.06	pH 5.5; Dose: 2 g/L; 25°C	This study
Untreated sawdust (general range)	Batch/Column	1.2-5.9	Variable (acidic pH typically)	Compiled from Ilyas et al., 2014; Ahmad et al., 2017; Haroon et al., 2025 [78-80]
Neem sawdust	Fixed-bed column	5.30	pH 2.0; Flow rate: 5 mL/min; Bed depth: 15 cm	Vinodhini & Das, 2010 [25]
Coconut shell charcoal	Fixed-bed column	4.83	pH 2.0; Flow rate: 10 mL/min; Bed depth: 10 cm	Babel & Kurniawan, 2004 [24]
Olive stone	Fixed-bed column	3.82	pH 2.0; Flow rate: 4 mL/min; Bed depth: 10 cm	Calero et al., 2016 [16]
Activated tamarind seeds	Fixed-bed column	4.75	pH 2.0; Flow rate: 5 mL/min; Bed depth: 15 cm	Gupta & Babu, 2010 [21]
Tea factory waste	Fixed-bed column	3.80	pH 2.0; Flow rate: 3 mL/min; Bed depth: 15 cm	Malkoc & Nuhoglu, 2006 [26]
Basalt rock	Fixed-bed column	14.0	pH 4.0; Flow rate: 4 mL/min; Bed depth: 20 cm	Kedir et al., 2025 [5]
Pomelo peel	Batch	0.57	pH 2.0; 25°C	Qiong Wang et al., 2020 [81]
Ferric chloride-modified pomelo peel	Batch	21.55	pH 2.0; 40°C	Qiong Wang et al., 2020 [81]
Citrus limetta peel	Batch	250	pH 2.0; Initial conc: 20 mg/L (not 20 g/L); 40°C	Saha et al., 2013 [82]

Notes:

The Citrus limetta capacity (250 mg/g) is exceptionally high and may reflect specific experimental conditions (a very high initial concentration or a unit conversion issue). The original paper [82] should be consulted for verification.

Basalt rock [5] hows higher capacity (14 mg/g) but is a mineral adsorbent, not biomass.

Modified adsorbents (e.g., ferric chloride-modified pomelo) show higher capacities but require additional chemicals and processing.

Direct comparison of adsorption capacities across studies must be interpreted with caution, as operating conditions (initial concentration, flow rate, bed depth, pH, temperature, particle size, and influent matrix) significantly influence reported capacities [83]. The values in Table 11 represent the maximum capacities reported under the specific conditions of each study and may not be directly comparable without considering these experimental variables. Where available, the operating conditions are provided in the table to facilitate meaningful comparison.

For example, higher initial concentrations typically yield higher apparent adsorption capacities due to increased driving force, while lower flow rates and deeper beds generally improve capacity. The comparison presented here is intended to position *Cordia africana* sawdust within the broader literature, not to claim superiority under all conditions.

3.11.1 Key Observations from the Comparison

- **Comparable Performance:** The raw *Cordia africana* sawdust (2.06 mg/g batch; 1.78 mg/g column) falls well within the 1.2-5.9 mg/g range reported for other unmodified sawdust materials. This confirms that it is neither exceptionally superior nor inferior to similar raw biomasses.
- **Removal Efficiency Advantage:** The removal efficiency observed for *Cordia africana* (60-84%) is notably higher than the typical 31-53% range reported for general unmodified sawdust. This suggests good surface-site accessibility despite the moderate absolute capacity.
- **Expected Batch vs. Column Difference:** The reduction from batch capacity (2.06 mg/g) to column capacity (1.78 mg/g) is approximately 14%, which is typical for fixed-bed systems due to mass-transfer limitations, shorter contact times, and non-ideal flow patterns.
- **Real Wastewater Penalty:** When tested with actual tannery wastewater, the column capacity dropped further to 1.51 mg/g (an ~15% reduction from synthetic solution performance), demonstrating the negative impact of competing ions (Cu^{2+}, Zn^{2+}, Fe^{3+}), high TDS, and COD.
- **pH Dependency Consideration:** Many literature studies achieved higher capacities (3.66 mg/g) at pH 2.0-3.0, where Cr(VI) exists predominantly as $HCrO_4^-$ and surface protonation is maximized [78-83]. This study operated at pH 5.5 (optimized for practical application and adsorbent stability), which is less aggressive but more realistic for industrial use.
- **Practical Implication:** While the capacity of raw sawdust is lower than modified or activated adsorbents, its negligible cost ($0.10-0.15 USD/kg) and locally available nature make it viable for low-budget or emergency applications, particularly for polishing Cr(VI)-contaminated water to meet regulatory discharge limits.

3.12 Statistical Significance of Operating Parameters

ANOVA results confirmed significant effects of both flow rate and bed depth on breakthrough time ($p < 0.01$ for both factors) and dynamic adsorption capacity ($p < 0.05$ for flow rate; $p < 0.01$ for bed depth). Tukey's HSD post-hoc analysis revealed that the 5 mL/min flow rate produced significantly longer breakthrough times than both 8 mL/min ($p = 0.008$) and 10 mL/min ($p = 0.003$) at 12 cm bed depth. Similarly, the 12 cm bed depth significantly outperformed the 6 cm bed depth ($p = 0.002$) and 9 cm bed depth ($p = 0.041$) at 5 mL/min. However, differences in q_e between 5 mL/min and 10 mL/min at 12 cm bed depth were not statistically significant ($p = 0.087$), indicating that the apparent increase in q_e at higher flow rates should be interpreted with caution. Table 12 presents 95% confidence intervals for key parameters.

Table 12 95% Confidence Intervals for Key Column Parameters (Run 7).

Parameter	Mean ± SD	95% CI
t_b (min)	50.0 ± 1.2	47.0-53.0
q_e (mg/g)	1.34 ± 0.04	1.28-1.40
MTZ (cm)	7.00 ± 0.18	6.55-7.45
Thomas q_0 (mg/g)	1.51 ± 0.04	1.44-1.58
Yoon-Nelson τ (min)	52.0 ± 1.3	48.8-55.2

3.13 Techno-Economic Considerations

The economic viability of any adsorbent depends on material costs, preparation requirements, regeneration potential, and disposal considerations. For raw *Cordia africana* sawdust, the following cost analysis is provided based on local market conditions in Ethiopia (2024 prices) and the experimental dynamic adsorption capacity of 1.78 mg/g under optimal conditions (Run 9: 12 cm bed depth, 10 mL/min flow rate).

It is important to emphasize that this analysis represents preliminary screening-level cost estimation rather than a comprehensive economic assessment. Actual costs for full-scale implementation would require detailed engineering design, site-specific labor rates, energy costs, regulatory compliance expenses, and capital equipment depreciation.

3.13.1 Direct Material and Preparation Costs

Direct material and preparation costs are presented in Table 13 below and cost comparison for alternative adsorbents in the Ethiopian market is presented in Table 14.

Table 13 Material costs.

Component	Cost (USD/kg)	Notes
Raw sawdust collection	$0.08-0.12	Local wood processing workshops
Sieving (labor)	Included above	Manual screening
Water washing	$0.01	Tap water
Drying	Negligible	Solar drying
Storage	$0.01	Polyethylene containers
Total preparation cost	$0.10-0.15	No chemical modification

Table 14 Cost comparison with commercial alternatives (Ethiopian market).

Adsorbent Type	Cost (USD/kg)	Notes
Raw *Cordia africana* sawdust	$0.10-0.15	This study
Commercial activated carbon (imported)	$1.50-2.50	Powdered or granular
Locally produced activated carbon	$0.80-1.20	Limited availability
Chemically modified adsorbents	$0.80-1.50	Excluding modification chemicals
Chitosan-based adsorbents	$15-25	Imported
Ion exchange resins	$20-50	Imported

3.13.2 Direct Treatment Cost Estimation

Base Case (No Regeneration):

Based on dynamic capacity of 1.78 mg/g under optimal conditions (Run 9: 12 cm bed depth, 10 mL/min flow rate, 47 mg/L Cr(VI)):

- Cr(VI) mass to be treated per 1000 L = 47 mg/L × 1000 L = 47,000 mg (47 g)
- Adsorbent required per 1000 L = 47,000 mg ÷ 1.78 mg/g = 26,404 g ≈ 26.4 kg
- Material cost per 1000 L treated: 26.4 kg × $0.10-0.15 USD/kg = $2.64-$3.96 USD

With Three-Cycle Reuse (76% Capacity Retention):

- Effective capacity over three cycles (average) = 1.78 mg/g × 0.76 = 1.35 mg/g
- Adjusted adsorbent required per 1000 L = 47,000 mg ÷ 1.35 mg/g = 34.8 kg
- Adjusted material cost per 1000 L (spread over 3 cycles) = 34.8 kg × $0.10-0.15 USD/kg ÷ 3 cycles = $1.16-$1.74 USD per 1000 L treated

3.13.3 Complete Cost Breakdown

The complete cost Breakdown to treat 1000 L of wastewater is presented in Table 15 below.

Table 15 Comprehensive Treatment Cost Breakdown (USD per 1000 L treated).

Cost Component	Without Regeneration	With 3-Cycle Reuse	Notes
Direct treatment costs			
Adsorbent material	\$2.64-3.96	\$1.16-1.74	Based on 1.78 mg/g capacity
pH adjustment (acid/base)	\$0.50-1.00	\$0.50-1.00	Adjusting pH 8.55 → 5.5 and back to pH 6-9
Pumping energy	\$0.15-0.30	\$0.15-0.30	Based on 0.5-1.0 kWh/m^3 at \$0.10/kWh
Labor (operator)	\$0.50-1.00	\$0.50-1.00	Based on 2-4 hours/day at \$5/hour
Regeneration costs			
HCl (0.1 M) consumption	-	\$0.30-0.50	Per regeneration cycle
Water rinsing	-	\$0.10-0.20	Distilled water for rinsing
Waste management			
Spent adsorbent disposal	\$5.28-10.56	\$2.32-4.64	Stabilization in cement/construction
Hazardous waste transport	\$1.00-2.00	\$1.00-2.00	Per 1000 L treated
Compliance and monitoring			
Effluent testing (Cr(VI), pH)	\$0.50-1.00	\$0.50-1.00	Laboratory analysis
Regulatory reporting	\$0.25-0.50	\$0.25-0.50	Documentation and permits
Total estimated cost	\$10.82-20.82	\$6.53-12.58	
Total cost per kg Cr(VI) removed	\$230-443	\$139-268	Based on 47 g Cr(VI)/1000 L

Note on treatment volume: The cost per 1000 L treated is based on 47 mg/L Cr(VI) concentration. For wastewater with higher or lower chromium concentrations, costs would scale accordingly (higher concentration = more adsorbent required per volume, but more chromium removed per volume).

3.13.4 Disposal Considerations

Spent adsorbent containing 1.78 mg/g chromium would require disposal as hazardous waste in many jurisdictions. Several options exist, the options and their costs are presented in Table 16.

Table 16 Disposal Options.

Disposal Option	Estimated Cost (USD/kg)	Feasibility
Stabilization in cement	$0.20-0.40	Technically feasible; requires testing
Incorporation in construction materials	$0.15-0.30	Potential for beneficial reuse; requires regulatory approval
Controlled incineration with recovery	$0.50-1.00	Requires further study; energy recovery potential
Secure landfill disposal	$0.10-0.20	Simple but may pose long-term environmental risk
Acid regeneration + recovery	$0.30-0.60	Could recover chromium value; requires further study

Disposal cost estimation (stabilization in cement):

• Without regeneration: $0.20-0.40 × 26.4 kg = $5.28-10.56 per 1000 L

• With 3-cycle reuse: $0.20-0.40 × 11.6 kg = $2.32-4.64 per 1000 L

Note: Stabilization in cement or construction materials would require verification of chromium leaching (TCLP testing) to confirm environmental safety. This cost does not include testing or regulatory approval fees.

3.13.5 Comparison with Conventional Technologies

Table 17 presents the comparison of adsorption with *Cordial africana* sawdust with other conventional technologies.

Table 17 Comparison with Conventional Technology.

Technology	Estimated Cost (USD/1000 L)	Advantages	Disadvantages
Raw *C. africana* sawdust	$6.53-20.82	Low cost, locally available, simple	Lower capacity, disposal issues
Activated carbon	$5-15	Well-established, high capacity	Higher material cost, energy-intensive regeneration
Ion exchange	$8-20	High efficiency, reusable resins	Higher capital cost, chemical consumption
Chemical precipitation	$3-10	Simple, low capital	Produces large sludge volume
Membrane filtration (RO/NF)	$10-30	High removal efficiency	High energy, membrane fouling

Source: Adapted from Bailey et al. (1999) [74] and Patel (2019) [48] with adjustments for Ethiopian market conditions.

Important caveat: The raw sawdust cost appears competitive with activated carbon and chemical precipitation. However, the substantially lower capacity (1.78 mg/g vs. 50-200 mg/g for activated carbon) means raw sawdust requires much more adsorbent mass per volume treated. This makes it less attractive for high-concentration Cr(VI) wastewater but potentially viable for polishing applications where Cr(VI) concentrations are low (<20 mg/L) and the cost of adsorbent replacement is acceptable.

3.13.6 Economic Viability Assessment

Best-Case Scenario (Low Concentration, High Efficiency):

- Wastewater Cr(VI) concentration: 10 mg/L
- Adsorbent capacity: 1.78 mg/g (optimistic)
- Treated volume per kg adsorbent: 1.78 mg/g ÷ 10 mg/L = 178 L/kg
- Material cost: $0.10-0.15/kg ÷ 178 L/kg = $0.56-0.84 per 1000 L
- Including other costs (disposal, labor, etc.): ~$3-5 per 1000 L

Worst-Case Scenario (High Concentration, Low Efficiency):

- Wastewater Cr(VI) concentration: 100 mg/L
- Adsorbent capacity: 1.34 mg/g (conservative, 3-cycle average)
- Treated volume per kg adsorbent: 1.34 mg/g ÷ 100 mg/L = 13.4 L/kg
- Material cost: $0.10-0.15/kg ÷ 13.4 L/kg = $7.46-11.19 per 1000 L
- Including other costs: ~$15-25 per 1000 L

Break-Even Concentration Analysis:

At $0.15/kg adsorbent, $0.30/kg disposal cost, and assuming 50% of cost is material and 50% is other operating costs:

Break-even with activated carbon ($10/1000 L total cost):

- Adsorbent cost contribution: ~$5/1000 L
- Adsorbent required: 5/0.15 = 33.3 kg
- Cr(VI) capacity: 33.3 kg × 1.78 mg/g = 59.3 g
- Break-even Cr(VI) concentration: 59.3 g/1000 L = 59 mg/L

Interpretation: Raw *Cordia africana* sawdust becomes economically competitive with activated carbon at Cr(VI) concentrations below approximately 50-60 mg/L. At higher concentrations, the high adsorbent mass requirement makes it less economically attractive than higher-capacity adsorbents.

3.13.7 Omitted Cost Components and Limitations

Table 18 presents the omitted cost during analysis.

Table 18 omitted cost.

Omitted Cost	Reason for Omission	Estimated Potential Impact
Capital equipment depreciation	Site- and scale-dependent	Could add $0.50-5.00 per 1000 L
Facility overhead	Site- and scale-dependent	Could add $0.50-2.00 per 1000 L
Emergency response planning	Regulatory requirement	Could add $0.10-0.50 per 1000 L
Regulatory permitting fees	Jurisdiction-dependent	Variable; could be significant
Worker training and PPE	Safety requirement	Could add $0.20-1.00 per 1000 L
Transportation of adsorbent	Location-dependent	Could add $0.50-2.00 per 1000 L
Sludge handling (beyond disposal)	Treatment requirement	Could add $0.50-1.00 per 1000 L
Contingency (10-20%)	Engineering practice	Could add 10-20% to total cost
Post-treatment pH adjustment	Discharge requirement	Could add $0.25-0.50 per 1000 L
Analytical QA/QC program	Regulatory compliance	Could add $0.25-0.50 per 1000 L

Acknowledged limitation: This techno-economic analysis is based on laboratory-scale data and Ethiopian local prices. The relatively low dynamic capacity (1.78 mg/g) suggests that raw *Cordia africana* sawdust may be more suitable for low-concentration Cr(VI) polishing applications or as an emergency treatment option rather than as a primary treatment for moderate-to-high Cr(VI) concentrations (>50 mg/L). Scale-up to industrial applications would require site-specific cost assessments for capital equipment, labor, energy, transportation, and regulatory compliance. Chemical modification or activation should be explored to improve capacity while maintaining cost-effectiveness.

The economic conclusions should therefore be interpreted as preliminary screening estimates rather than definitive treatment costs. Pilot-scale studies and detailed engineering analysis would be required to establish realistic cost estimates for full-scale implementation.

3.13.8 Recommendations for Economic Optimization

1. Match adsorbent to application: Use raw sawdust for low-concentration Cr(VI) (<20 mg/L) polishing or emergency treatment; consider modification or alternative adsorbents for higher concentrations.
2. Optimize regeneration frequency: Based on breakthrough curves, determine the optimal cycle length that balances capacity utilization vs. regeneration costs. The data suggest 50-80 minutes of operation time depending on flow rate and bed depth.
3. Explore beneficial reuse of spent adsorbent: Investigate incorporation into construction materials or stabilization in cement to offset disposal costs and recover value.
4. Consider local availability: Transport costs can significantly impact total cost; prioritize local sourcing and application.
5. Scale-up economics: Larger column diameters and multiple columns in series may improve efficiency and reduce per-volume costs.

6. Investigate chemical modification: Low-cost modifications (e.g., acid treatment, base treatment) could improve capacity with modest cost increases.

4. Conclusion

This study systematically examined the dynamic adsorption performance of raw *Cordia africana* sawdust for the removal of hexavalent chromium from aqueous solution and real tannery wastewater in a fixed-bed column system. Based on the experimental results obtained with proper replication and statistical analysis, the following conclusions can be drawn:

1. Operating parameters significantly impact column performance: Lower flow rates (5 mL/min) and greater bed depths (12 cm) provide improved breakthrough time and bed utilization efficiency. Breakthrough time increased from 36.0 to 50.0 min as flow rate decreased from 10 to 5 mL/min at 12 cm bed depth, while increasing bed depth from 6 to 12 cm at 5 mL/min extended breakthrough time from 30.0 to 50.0 min.
2. Chromium speciation reveals coupled adsorption-reduction mechanism: During the adsorption process, partial reduction of Cr(VI) to Cr(III) occurred, with approximately 28% of adsorbed chromium present as Cr(III) on the spent adsorbent. This transformation represents a detoxification pathway but may contribute to gradual capacity loss during regeneration.
3. The adsorbent demonstrates competitive adsorption capacity: Raw *Cordia africana* sawdust achieved a maximum dynamic adsorption capacity of 1.78 ± 0.06 mg/g for synthetic Cr(VI) solution under optimal conditions, with a batch capacity of 2.06 mg/g. This capacity falls within the typical range reported for unmodified sawdust materials (1.2-5.9 mg/g).
4. Kinetic models adequately describe breakthrough behavior: The Thomas, Yoon-Nelson, and BDST models showed good agreement with experimental data ($R^2 > 0.94$, RMSE < 1.84 mg/L), confirming their applicability for describing fixed-bed adsorption behavior.
5. The adsorbent exhibits moderate regeneration potential: Three consecutive adsorption-desorption cycles showed gradual capacity loss, with approximately 76% of initial capacity retained after the third cycle.
6. Practical potential with real wastewater is demonstrated: When applied to real tannery wastewater containing competing ions, high TDS, and elevated COD, the adsorbent achieved a dynamic capacity of 1.51 ± 0.28 mg/g, representing approximately 85% of the capacity observed with synthetic solution.
7. Preliminary economic advantages are evident: Treatment costs are estimated at $7.92-14.52 USD per 1000 L without regeneration or $8.12-15.66 USD per 1000 L with three-cycle reuse, which is comparable to or lower than conventional technologies.

In summary, raw *Cordia africana* sawdust shows preliminary promise as an effective, low-cost, and environmentally friendly adsorbent for the removal of hexavalent chromium from polluted water in continuous flow systems. Its moderate but competitive adsorption capacity (1.78 mg/g), reasonable regeneration potential (76% after three cycles), and successful application to real industrial wastewater (1.51 mg/g) support its consideration for polishing applications of low-to-moderate Cr(VI) concentrations or as an emergency treatment option in resource-limited settings where conventional treatment technologies may not be economically feasible.

However, the following critical limitations must be acknowledged before any practical application:

- The study remains at laboratory scale; pilot-scale validation is required before full-scale implementation.
- Only three regeneration cycles were evaluated; long-term stability over 10-20 cycles is unknown.
- Post-regeneration characterization (FTIR, SEM, BET) was not performed, so mechanisms of capacity loss remain speculative.
- XPS and EPR analyses were not conducted, so the reduction mechanism cannot be definitively confirmed.
- Spent adsorbent disposal and leaching characteristics (TCLP, SPLP) were not assessed.
- Mechanical durability (particle attrition, pressure-drop development) after repeated regeneration was not evaluated.
- The techno-economic analysis is based on simplified assumptions and local prices; comprehensive cost assessment is required.
- Regulatory compliance for treated effluent (discharge limits) was not confirmed.
- The comparison between synthetic and real wastewater was not concentration-matched (47 mg/L vs. 35 mg/L).
- Model assumptions (axial dispersion, surface reaction control, Langmuir kinetics) were not independently verified.

The practical implications should therefore be framed as preliminary laboratory-scale feasibility rather than demonstrated deployment readiness.

5. Recommendations for Future Work

Based on the findings of this study, the following recommendations are suggested for future research:

1. Pilot-scale studies: Scale-up studies using larger columns (diameter >5 cm, bed depth >50 cm) and continuous operation should be conducted to confirm laboratory findings and generate design parameters.
2. Long-term stability assessment: Longer operation studies over 10-20 adsorption-desorption cycles would provide a better understanding of long-term adsorbent stability and replacement frequency requirements. Post-regeneration characterization (FTIR, SEM, BET) should be included.
3. Disposal and resource recovery: Investigation of safe disposal methods for spent adsorbent and potential recovery of adsorbed chromium. Leaching tests (TCLP or equivalent) should be conducted to assess environmental safety.
4. Regulatory compliance: Treated effluent should be evaluated against Ethiopian and international discharge standards (total Cr <2 mg/L, Cr(VI) <0.1 mg/L where applicable).
5. Surface modification studies: Controlled chemical modification using environmentally benign agents could improve adsorption capacity, but must be weighed against increased costs and environmental impacts.
6. Breakthrough curve modeling: Comprehensive models that account for axial dispersion, film mass transfer, and intraparticle diffusion should be developed and validated.

7. Multi-component adsorption studies: Systematic investigation of competitive adsorption in well-defined multi-metal systems would provide insight into selectivity and competition mechanisms.
8. Concentration-matched real wastewater studies: Future studies should conduct experiments with real wastewater spiked or diluted to match the synthetic solution concentration (47 mg/L Cr(VI)) to isolate matrix effects from concentration effects.
9. Life Cycle Assessment (LCA): Comprehensive LCA comparing raw sawdust with conventional technologies (activated carbon, ion exchange, chemical precipitation) to quantify environmental benefits.

Author Contributions

Aster Woldu Gebrearegay: Conceptualization, methodology, investigation, formal analysis, writing – original draft, visualization. Melaku Tesfaye: Supervision, validation, resources, data curation, writing – review & editing, project administration. Alemu Gizaw: Supervision, validation, formal analysis, writing – review & editing. All authors have read and agreed to the published version of the manuscript.

Competing Interests

The authors have declared that no competing interests exist.

AI-Assisted Technologies Statement

We wish to transparently disclose that AI language tools (ChatGPT-4) were used solely to polish the English language and improve the readability of certain sections of this manuscript. All scientific content, experimental data, analysis, interpretations, and conclusions are entirely original and the work of the authors. The AI assistance was limited to linguistic refinement and did not contribute to the research design, data collection, data analysis, or intellectual content. We have carefully reviewed and verified every sentence to ensure accuracy and integrity.

Additional Materials

The following additional materials are uploaded at the page of this paper.

1. Table S1: Preliminary Batch Optimization Data for pH Effect on Cr(VI) Adsorption onto Raw *Cordia africana* Sawdust (Mean ± SD, n = 3).
2. Figure S1: Effect of solution pH on Cr(VI) removal efficiency and adsorption capacity of raw *Cordia africana* sawdust.

References

1. Sharma P, Singh SP, Parakh SK, Tong YW. Health hazards of hexavalent chromium (Cr(VI)) and its microbial reduction. Bioengineered. 2022; 13: 4923-4938.

2. Rajapaksha AU, Selvasembian R, Ashiq A, Gunarathne V, Ekanayake A, Perera VO, et al. A systematic review on adsorptive removal of hexavalent chromium from aqueous solutions: Recent advances. Sci Total Environ. 2022; 809: 152055.
3. Park D, Yun YS, Park JM. Reduction of hexavalent chromium with the brown seaweed *Ecklonia* biomass. Environ Sci Technol. 2004; 38: 4860-4864.
4. Baral SS, Das SN, Rath P. Hexavalent chromium removal from aqueous solution by adsorption on treated sawdust. Biochem Eng J. 2006; 31: 216-222.
5. Abdu KY, Endris YA, Shah MA. Chromium removal using a basalt rock adsorbent in a packed bed column for efficient environmental protection. ACS Omega. 2025; 10: 727-739.
6. Park JE, Shin JH, Oh W, Choi SJ, Kim J, Kim C, et al. Removal of hexavalent Chromium(VI) from wastewater using chitosan-coated iron oxide nanocomposite membranes. Toxics. 2022; 10: 98.
7. Bohart GS, Adams EQ. Some aspects of the behavior of charcoal with respect to chlorine. J Am Chem Soc. 1920; 42: 523-544.
8. Thomas HC. Heterogeneous ion exchange in a flowing system. J Am Chem Soc. 1944; 66: 1664-1666.
9. Yoon YH, Nelson JH. Application of gas adsorption kinetics I. A theoretical model for respirator cartridge service life. Am Ind Hyg Assoc J. 1984; 45: 509-516.
10. Golie WM, Upadhyayula S. Continuous fixed-bed column study for the removal of nitrate from water using chitosan/alumina composite. J Water Process Eng. 2016; 12: 58-65.
11. Du Z, Zheng T, Wang P. Experimental and modelling studies on fixed bed adsorption for Cu(II) removal from aqueous solution by carboxyl modified jute fiber. Powder Technol. 2018; 338: 952-959.
12. Ramirez A, Giraldo S, García-Nunez J, Flórez E, Acelas N. Phosphate removal from water using a hybrid material in a fixed-bed column. J Water Process Eng. 2018; 26: 131-137.
13. Foo KY, Hameed BH. Insights into the modeling of adsorption isotherm systems. Chem Eng J. 2010; 156: 2-10.
14. Kannan N, Sundaram MM. Kinetics and mechanism of removal of methylene blue by adsorption on various carbons-A comparative study. Dyes Pigm. 2001; 51: 25-40.
15. Tadesse I, Isoaho SA, Green FB, Puhakka JA. Removal of organics and nutrients from tannery effluent by advanced integrated wastewater pond systems technology. Water Sci Technol. 2003; 48: 307-314.
16. Calero M, Ronda A, Pérez A, Yáñez A, Trujillo MC, Martín-Lara MÁ. The scale-up of Cr^{3+} biosorption onto olive stone in a fixed bed column. Desalin Water Treat. 2016; 57: 25140-25152.
17. Lee CG, Kim JH, Kang JK, Kim SB, Park SJ, Lee SH, et al. Comparative analysis of fixed-bed sorption models using phosphate breakthrough curves in slag filter media. Desalin Water Treat. 2015; 55: 1795-1805.
18. Reinhardt T, Rott E, Schneider PA, Minke R, Schönberger H. Fixed-bed column studies of phosphonate and phosphate adsorption on granular ferric hydroxide (GFH). Process Saf Environ Prot. 2021; 153: 301-310.
19. Stuart TD, Ramarao BV. Breakthrough curve modeling for protein adsorption in fibrous depth filters using colloid filtration theory. Ind Eng Chem Res. 2025; 64: 14194-14207.
20. Pratap T, Chaubey AK, Kapoor S, Preetiva B, Mohan D. Fixed-bed adsorption system design models for groundwater nitrate removal using acid-modified biochar developed from invasive *Prosopis juliflora* bark. ACS Sustain Resour Manage. 2025; 2: 572-580.

21. Gupta S, Babu BV. Experimental investigations and theoretical modeling aspects in column studies for removal of Cr(VI) from aqueous solutions using activated tamarind seeds. J Water Resour Prot. 2010; 2: 706-716.
22. Liu Y, Shan H, Pang Y, Zhan H, Zeng C. Iron modified chitosan/coconut shell activated carbon composite beads for Cr(VI) removal from aqueous solution. Int J Biol Macromol. 2023; 224: 156-169.
23. Lissy PM, Madhu G, Thomas RM. Numerical modelling of a fixed bed column for the Cr(VI) adsorption using pyrrole coated nanocomposite. J Indian Chem Soc. 2025; 102: 101568.
24. Babel S, Kurniawan TA. Cr(VI) removal from synthetic wastewater using coconut shell charcoal and commercial activated carbon modified with oxidizing agents and/or chitosan. Chemosphere. 2004; 54: 951-967.
25. Vinodhini V, Das N. Packed bed column studies on Cr(VI) removal from tannery wastewater by neem sawdust. Desali24nation. 2010; 264: 9-14.
26. Malkoc E, Nuhoglu Y. Fixed bed studies for the sorption of chromium(VI) onto tea factory waste. Chem Eng Sci. 2006; 61: 4363-4372.
27. Han R, Wang Y, Zhao X, Wang Y, Xie F, Cheng J, et al. Adsorption of methylene blue by phoenix tree leaf powder in a fixed-bed column: Experiments and prediction of breakthrough curves. Desalination. 2009; 245: 284-297.
28. Garg UK, Kaur MP, Garg VK, Sud D. Removal of hexavalent chromium from aqueous solution by agricultural waste biomass. J Hazard Mater. 2007; 140: 60-68.
29. Suksabye P, Thiravetyan P, Nakbanpote W. Column study of chromium(VI) adsorption from electroplating industry by coconut coir pith. J Hazard Mater. 2008; 160: 56-62.
30. Taty-Costodes VC, Fauduet H, Porte C, Delacroix A. Removal of Cd(II) and Pb(II) ions, from aqueous solutions, by adsorption onto sawdust of Pinus sylvestris. J Hazard Mater. 2003; 105: 121-142.
31. Ruthven DM. Principles of adsorption and adsorption processes. Hoboken, NJ: John Wiley & Sons, Inc.; 1984.
32. McCabe WL, Smith JC, Harriott P. Unit operations of chemical engineering. 7th ed. New York, NY: McGraw Hill; 2005.
33. Babu BV, Gupta S. Modeling and simulation of fixed bed adsorption column: Effect of velocity variation. i-manager's J Future Eng Technol. 2005; 1: 60-66.
34. Ahmad AA, Hameed BH. Fixed-bed adsorption of reactive azo dye onto granular activated carbon prepared from waste. J Hazard Mater. 2010; 175: 298-303.
35. Eaton AD, Clesceri LS, Rice EW, Greenberg AE. Standard methods for the examination of water and wastewater. 21st ed. Washington, D.C.: APHA; 2005.
36. Miretzky P, Cirelli AF. Cr(VI) and Cr(III) removal from aqueous solution by raw and modified lignocellulosic materials: A review. J Hazard Mater. 2010; 180: 1-19.
37. Mohan D, Pittman Jr CU. Activated carbons and low cost adsorbents for remediation of tri- and hexavalent chromium from water. J Hazard Mater. 2006; 137: 762-811.
38. Baird RB, Eaton AD, Rice EW. Standard methods for the examination of water and wastewater. 23rd ed. Washington, D.C.: American Public Health Association; 2017.
39. Cooney DO. Adsorption design for wastewater treatment. Boca Raton, FL: CRC Press; 1999.
40. Weber Jr WJ, McGinley PM, Katz LE. Sorption phenomena in subsurface systems: Concepts, models and effects on contaminant fate and transport. Water Res. 1991; 25: 499-528.

41. Aksu Z, Gönen F. Biosorption of phenol by immobilized activated sludge in a continuous packed bed: Prediction of breakthrough curves. Process Biochem. 2004; 39: 599-613.
42. Volesky B, Weber J, Park JM. Continuous-flow metal biosorption in a regenerable *Sargassum* column. Water Res. 2003; 37: 297-306.
43. Chu KH. Improved fixed bed models for metal biosorption. Chem Eng J. 2004; 97: 233-239.
44. Vijayaraghavan K, Jegan J, Palanivelu K, Velan M. Biosorption of copper, cobalt and nickel by marine green alga *Ulva reticulata* in a packed column. Chemosphere. 2005; 60: 419-426.
45. Ko DCK, Porter JF, McKay G. Optimised correlations for the fixed-bed adsorption of metal ions on bone char. Chem Eng Sci. 2000; 55: 5819-5829.
46. Aksu Z. Application of biosorption for the removal of organic pollutants: A review. Process Biochem. 2005; 40: 997-1026.
47. Sperlich A, Schimmelpfennig S, Baumgarten B, Genz A, Amy G, Worch E, et al. Predicting anion breakthrough in granular ferric hydroxide (GFH) adsorption filters. Water Res. 2008; 42: 2073-2082.
48. Patel H. Fixed-bed column adsorption study: A comprehensive review. Appl Water Sci. 2019; 9: 45.
49. Xu Z, Cai JG, Pan BC. Mathematically modeling fixed-bed adsorption in aqueous systems. J Zhejiang Univ Sci A. 2013; 14: 155-176.
50. Borba CE, Guirardello R, Silva EA, Veit MT, Tavares CR. Removal of nickel(II) ions from aqueous solution by biosorption in a fixed bed column: Experimental and theoretical breakthrough curves. Biochem Eng J. 2006; 30: 184-191.
51. Cruz-Olivares J, Pérez-Alonso C, Barrera-Díaz C, Ureña-Nuñez F, Chaparro-Mercado MC, Bilyeu B. Modeling of lead(II) biosorption by residue of allspice in a fixed-bed column. Chem Eng J. 2013; 228: 21-27.
52. Hutchins RA. New method simplifies design of activated carbon systems. Chem Eng. 1973; 80: 133-138.
53. Sotelo JL, Ovejero G, Rodríguez A, Álvarez S, Galán J, García J. Competitive adsorption studies of caffeine and diclofenac aqueous solutions by activated carbon. Chem Eng J. 2014; 240: 443-453.
54. Tsai WT, Chang CY, Ho CY, Chen LY. Adsorption properties and breakthrough model of 1,1-dichloro-1-fluoroethane on activated carbons. J Hazard Mater. 1999; 69: 53-66.
55. Goel J, Kadirvelu K, Rajagopal C, Garg VK. Removal of lead(II) by adsorption using treated granular activated carbon: Batch and column studies. J Hazard Mater. 2005; 125: 211-220.
56. Naja G, Volesky B. Behavior of the mass transfer zone in a biosorption column. Environ Sci Technol. 2006; 40: 3996-4003.
57. Lodeiro P, Herrero R, de Vicente MS. Batch desorption studies and multiple sorption-regeneration cycles in a fixed-bed column for Cd(II) elimination by protonated *Sargassum muticum*. J Hazard Mater. 2006; 137: 1649-1655.
58. Chandra Srivastava V, Deo Mall I, Mani Mishra I. Modelling individual and competitive adsorption of Cadmium(II) and Zinc(II) metal ions from aqueous solution onto bagasse fly ash. Sep Sci Technol. 2006; 41: 2685-2710.
59. Singh S, Srivastava VC, Mall ID. Fixed-bed study for adsorptive removal of furfural by activated carbon. Colloids Surf A Physicochem Eng Asp. 2009; 332: 50-56.

60. Gupta VK, Rastogi A, Nayak A. Biosorption of nickel onto treated alga (*Oedogonium hatei*): Application of isotherm and kinetic models. J Colloid Interface Sci. 2010; 342: 533-539.
61. Kratochvil D, Pimentel P, Volesky B. Removal of trivalent and hexavalent chromium by seaweed biosorbent. Environ Sci Technol. 1998; 32: 2693-2698.
62. Kumar PA, Chakraborty S. Fixed-bed column study for hexavalent chromium removal and recovery by short-chain polyaniline synthesized on jute fiber. J Hazard Mater. 2009; 162: 1086-1098.
63. Babu BV, Gupta S. Adsorption of Cr(VI) using activated neem leaves: Kinetic studies. Adsorption. 2008; 14: 85-92.
64. Han R, Zhang J, Zou W, Shi J, Liu H. Equilibrium biosorption isotherm for lead ion on chaff. J Hazard Mater. 2005; 125: 266-271.
65. Sharma N, Kaur K, Kaur S. Kinetic and equilibrium studies on the removal of Cd^{2+} ions from water using polyacrylamide grafted rice (*Oryza sativa*) husk and (*Tectona grandis*) saw dust. J Hazard Mater. 2009; 163: 1338-1344.
66. Vijayaraghavan K, Yun YS. Bacterial biosorbents and biosorption. Biotechnol Adv. 2008; 26: 266-291.
67. Chowdhury Z, Zain SM, Rashid AK. Equilibrium isotherm modeling, kinetics and thermodynamics study for removal of lead from waste water. J Chem. 2011; 8: 333-339.
68. Tan IA, Ahmad AL, Hameed BH. Adsorption of basic dye using activated carbon prepared from oil palm shell: Batch and fixed bed studies. Desalination. 2008; 225: 13-28.
69. Al-Degs YS, Khraisheh MA, Allen SJ, Ahmad MN. Adsorption characteristics of reactive dyes in columns of activated carbon. J Hazard Mater. 2009; 165: 944-949.
70. Sharma PK, Ayub S, Tripathi CN. Agro and horticultural wastes as low cost adsorbents for removal of heavy metals from wastewater: A review. Int Ref J Eng Sci. 2013; 2: 18-27.
71. Sharma YC, Srivastava V, Srivastava J, Mahto M. Reclamation of Cr(VI) rich water and wastewater by wollastonite. Chem Eng J. 2007; 127: 151-156.
72. World Health Organization. Guidelines for drinking-water quality. 4th ed. Geneva, Switzerland: WHO; 2011.
73. Volesky B. Biosorption and me. Water Res. 2007; 41: 4017-4029.
74. Bailey SE, Olin TJ, Bricka RM, Adrian DD. A review of potentially low-cost sorbents for heavy metals. Water Res. 1999; 33: 2469-2479.
75. Park D, Yun YS, Park JM. Studies on hexavalent chromium biosorption by chemically-treated biomass of *Ecklonia* sp. Chemosphere. 2005; 60: 1356-1364.
76. Demirbas A. Heavy metal adsorption onto agro-based waste materials: A review. J Hazard Mater. 2008; 157: 220-229.
77. Sud D, Mahajan G, Kaur MP. Agricultural waste material as potential adsorbent for sequestering heavy metal ions from aqueous solutions-A review. Bioresour Technol. 2008; 99: 6017-6027.
78. Ilyas M, Ahmad A, Ghazi ZA, Sohail M, Arif M, Khan ZU. Investigation of the activity of sawdust as biosorbent towards Cr(VI) removal from waste water: Kinetic and thermodynamic studies. Int J Environ Sci. 2014; 3: 5-12.
79. Ahmad A, Ghazi ZA, Saeed M, Ilyas M, Ahmad R, Muqsit Khattak A, et al. A comparative study of the removal of Cr(VI) from synthetic solution using natural biosorbents. New J Chem. 2017; 41: 10799-10807.

80. Haroon H, Butt TA, Shah JA, Ciobica A, Romila LE, Burlui V, et al. Valorization of natural adsorbents for removing chromium(VI) from industrial wastewater: A review. Front Chem. 2025; 13: 1608863.
81. Wang Q, Zhou C, Kuang YJ, Jiang ZH, Yang M. Removal of hexavalent chromium in aquatic solutions by pomelo peel. Water Sci Eng. 2020; 13: 65-73.
82. Saha R, Mukherjee K, Saha I, Ghosh A, Ghosh SK, Saha B. Removal of hexavalent chromium from water by adsorption on mosambi (*Citrus limetta*) peel. Res Chem Intermed. 2013; 39: 2245-2257.
83. Ho YS, McKay G. Pseudo-second order model for sorption processes. Process Biochem. 1999; 34: 451-465.